Since January 2020 Elsevier has created a COVID-19 resource centre with free information in English and Mandarin on the novel coronavirus COVID-19. The COVID-19 resource centre is hosted on Elsevier Connect, the company's public news and information website.

Computational Biology and Chemistry 98 (2022) 107645

Contents lists available at ScienceDirect

Computational Biology and Chemistry

journal homepage: www.elsevier.com/locate/cbac

A global report on the dynamics of COVID-19 with quarantine and hospitalization: A fractional order model with non-local kernel

Zubair Ahmad [a], Sherif A. El-Kafrawy [b,c], Thamir A. Alandijany [b,c], Francesco Giannino [d], Ahmed A. Mirza [b,c], Mai M. El-Daly [b,c], Arwa A. Faizo [b,c], Leena H. Bajrai [b,e], Mohammad Amjad Kamal [b,f,g,h], Esam I. Azhar [b,c,*]

[a] Dipartimento di Matematica e Fisica, Universit'a degli Studi della Campania "Luigi Vanvitelli", Caserta 81100, Italy
[b] Special Infectious Agents Unit, King Fahd Medical Research Center, King Abdulaziz University, Jeddah, Saudi Arabia
[c] Department of Medical Laboratory Sciences, Faculty of Applied Medical Sciences, King Abdulaziz University, Jeddah, Saudi Arabia
[d] Department of Agricultural Sciences, University of Naples Federico II, Portici, Italy
[e] Biochemistry Department, Faculty of Sciences, King Abdulaziz University, Jeddah, Saudi Arabia
[f] Institutes for Systems Genetics, Frontiers Science Center for Disease-related Molecular Network, West China Hospital, Sichuan University, Chengdu 610041, Sichuan, China
[g] Department of Pharmacy, Faculty of Allied Health Sciences, Daffodil International University, Bangladesh
[h] Enzymoics, 7 Peterlee place, Novel Global Community Educational Foundation, Hebersham, NSW 2770, Australia

ARTICLE INFO

Keywords:
COVID-19
Atangana-Baleanu (ABC) Fractional Derivative
MATLAB
Basic Reproduction Number
Disease Free Equilibrium
Endemic Equilibrium

ABSTRACT

In this paper, a compartmental mathematical model has been utilized to gain a better insight about the future dynamics of COVID-19. The total human population is divided into eight various compartments including susceptible, exposed, pre-asymptomatic, asymptomatic, symptomatic, quarantined, hospitalized and recovered or removed individuals. The problem was modeled in terms of highly nonlinear coupled system of classical order ordinary differential equations (ODEs) which was further generalized with the Atangana-Balaeanu (ABC) fractional derivative in Caputo sense with nonlocal kernel. Furthermore, some theoretical analyses have been done such as boundedness, positivity, existence and uniqueness of the considered. Disease-free and endemic equilibrium points were also assessed. The basic reproduction was calculated through next generation technique. Due to high risk of infection, in the present study, we have considered the reported cases from three continents namely Americas, Europe, and south-east Asia. The reported cases were considered between 1st May 2021 and 31st July 2021 and on the basis of this data, the spread of infection is predicted for the next 200 days. The graphical solution of the considered nonlinear fractional model was obtained via numerical scheme by implementing the MATLAB software. Based on the fitted values of parameters, the basic reproduction number $\Re_0$ for the case of America, Asia and Europe were calculated as $\Re_0 \approx 2.92819$, $\Re_0 \approx 2.87970$ and $\Re_0 \approx 2.23507$ respectively. It is also observed that the spread of infection in America is comparatively high followed by Asia and Europe. Moreover, the effect of fractional parameter is shown on the dynamics of spread of infection among different classes. Additionally, the effect of quarantined and treatment of infected individuals is also shown graphically. From the present analysis it is observed that awareness of being quarantine and proper treatment can reduce the infection rate dramatically and a minimal variation in quarantine and treatment rates of infected individuals can lead us to decrease the rate of infection.

1. Introduction

COVID-19 affected many countries in terms of public health and economy (Bendavid et al., 2021). In the last couple of months, several SARS-CoV-2 variants have been emerged with some of them demonstrating active circulation and transmission dynamics (Khan and

* Corresponding author at: Special Infectious Agents Unit, King Fahd Medical Research Center, King Abdulaziz University, Jeddah, Saudi Arabia.
E-mail addresses: xubair5383@gmail.com (Z. Ahmad), saelkfrawy@kau.edu.sa (S.A. El-Kafrawy), talandijany@kau.edu.sa (T.A. Alandijany), giannino@unina.it (F. Giannino), amirza1@kau.edu.sa (A.A. Mirza), meldaly@kau.edu.sa (M.M. El-Daly), aafaizo@kau.edu.sa (A.A. Faizo), lbajrai@kau.edu.sa (L.H. Bajrai), prof.ma.kamal@gmail.com (M.A. Kamal), eazhar@kau.edu.sa (E.I. Azhar).

https://doi.org/10.1016/j.compbiolchem.2022.107645
Received 15 October 2021; Received in revised form 15 February 2022; Accepted 16 February 2022
Available online 19 February 2022

Atangana, 2020; SÁNCHEZ et al., 2020). Predicting and understanding the future viral transmission is key for infection control and prevention (Burki, 2020; Jin et al., 2020; Pellis et al., 2021; Zhao and Chen, 2020). Mathematical models are precious tools for this purpose. Indeed, different types of mathematical models with different fractional derivatives are utilized to investigate the dynamics and control of COVID-19 (Grassly et al., 2020; Grigorieva et al., 2020; Kassa et al., 2020; Memon et al., 2021). Many studies are reported for the dynamics and forecasting of COVID-19 by considering real data of different regions. Like, the early dynamics and clinical severity of COVID-19 in China by using mathematical tools can be seen in (Kucharski et al., 2020; Wu et al., 2020). Similarly, mathematical modeling and forecasting with intervention strategies, social media advertisement, isolation, quarantine, community awareness, global information compaigns with the consideration of real data from India in order to predict the future scenario of the disease can be seen in (Khajanchi et al., 2020, 2021b; Khajanchi and Sarkar, 2020; Rai et al., 2022; Samui et al., 2020; Sarkar et al., 2020; Tiwari et al., 2021).

Fractional derivative is a powerful tool to discuss the complexity of the physical and engineering problems. Observations indicates that some physical phenomenon cannot be explained properly through classical order derivatives. Non-integer order derivatives are proven to be a best tool to best fit the theoretical results with the real data (Qureshi and Atangana, 2019; Yavuz and Özdemir, 2019; Yusuf et al., 2020). The applications and uses of fractional derivatives can be seen in different physical, engineering and health sciences such as sustainable energy, fluid mechanics, infectious disease modeling, biochemistry, electrical circuits and so on (Z. Ahmad et al., 2020b, 2021; AHMAD et al., 2021; AHMAD et al., 2021; AHMAD et al., 2021; AHMAD et al., 2021; Ali et al., 2020; Murtaza et al., 2022; Sinan et al., 2022). Besides this, previous work reported on the fractional dynamics of COVID-19 which is proved to be best fit with the real data. The reported study indicates that fractional models with power law kernel, exponential kernel or Mittag-Leffler kernel gives us best results as compared to classical models. Yadav and Verma investigated the transmission of COVID-19 in Wuhan China by using fractional derivatives (Yadav and Renu Verma, 2020). They observed that the real data can be best fit in case of fractional order derivative. Rajagopal et al. investigated the spread of COVID-19 in Italy (Rajagopal et al., 2020). They compared the results for the case of integer and non-integer derivative and found less error with the real data for the case of fractional derivative. Nisar et al. predicted the spread of COVID-19 via fractional derivatives (Nisar et al., 2021). They compared their model's results with the real data of Wuhan China for initial days.

Some physical problems obey power law while some satisfy exponential law. Reported studies indicates that epidemiological problems can be best explain with the exponential laws because it obeys exponential laws. The fractional differential operators having exponential or Mittag-Leffler kernels can best explain the problems concerned with exponential laws. Due to the cross-over behavior, the fractional operator having Mittag-Leffler kernel i.e., Atangana-Baleanu fractional differential operator can best explain the complex dynamics of epidemiological problems (Abdullah et al., 2021; Abdullah et al., 2021; Abdullah et al., 2021; Abdullah et al., 2021; S. Ahmad et al., 2020; Z. Ahmad et al., 2020a; Arfan et al., 2021; Naik et al., 2020; Qureshi et al., 2019a, 2019b; Qureshi and Yusuf, 2019b, 2019a; Shah et al., 2020; Shatanawi et al., 2021). Qureshi et al. predicted the transmission of varicella zoster virus via different fractional operators i.e., Caputo, Caputo Fabrizio (CF) and Atangana-Baleanu (AB) fractional operators (Qureshi et al., 2019b). They found that AB fractional derivative gives the highest performance as compared to the rest of fractional derivatives. Similarly, it was reported the comparison of different fractional operators for the dynamics of diarrhea and found that AB fractional derivative gives the outstanding performance (Qureshi et al., 2019a). Qureshi and Yusuf reported the dynamics of chicken pox disease among the children in Schenzen city of China (Qureshi and Yusuf, 2019a, 2019b). They investigated their results by generalizing the classical model through different fractional derivatives and found that the dynamics can be best explain with AB fractional differential operator. Ahmad et al. analyzed the dynamics of COVID-19 in Pakistan by using AB fractional derivative (Z. Ahmad et al., 2020a). Naik et al. investigated the future scenario of COVID-19 in Pakistan by using different fractional operators and they noticed that AB fractional derivative gives us the highest efficiency rate with the real data (Naik et al., 2020). In the same way, Arfan et al. utilized the generalized Euler method for the results of fractional order COVID-19 model to predict the spread of COVID-19 in Pakistan (Arfan et al., 2021). Shatanawi et al. analyzed the spread of TB in Yemen for the period between 2000 and 2019 by using generalized AB fractional operator (Shatanawi et al., 2021). Shah et al. forecast the spread of COVID-19 using factional derivative by implementing Adomian decomposition technique (Shah et al., 2020). The modified Euler method was utilized by Ahmad et al. for the solution of the fractional order COVID-19 model in order to forecast the transmission of COVID-19 in Wuhan, China (S. Ahmad et al., 2020). Similarly, Abdullah et al. analyzed the transmission of COVID-19 in Wuhan, China under the consideration of fractional derivative (Abdullah et al., 2021; Abdullah et al., 2021; Abdullah et al., 2021; Abdullah et al., 2021). Shaikh et al. analyzed fractional order COVID-19 model for the spread and control of COVID-19 in India (Shaikh et al., 2020). Singh et al. reported the stability analysis and numerical investigation of the non-integer COVID-19 model (Singh et al., 2021). Danane et al. studied the numerical analysis of the stochastic COVID-19 model with the Levy noise model (Danane et al., 2021).

The main concern of epidemiological models is to find some possible ways to vanish or minimize the spread of infection. For this, the optimal control is proved to be a best tool and is applied to many infectious disease problems. Sharomi and Malik studied some applications of optimal control in epidemiological problems (Sharomi and Malik, 2017). Agusto and Khan reported the spread of dengue infection with the implementation of optimal control strategies and found that optimal control can drastically reduce the transmission of illness (Agusto and Khan, 2018). Sinan et al. reported the analysis for the transmission of malaria disease with optimal control and observed that optimal control such as spray of insecticides or proper treatment can quickly reduce the disease spread (Sinan et al., 2022). Ali et al. reported the optimal control of zika virus disease with the fractional derivatives (Ali et al., 2022a, 2022b). Similarly the utilization of the idea of optimal control for the control of COVID-19 can be seen in (Aba Oud et al., 2021; S. W. Abdullah Ahmad et al., 2021; S.W. Ahmad et al., 2021; z Ahmad et al., 2021; Z. Ahmad et al., 2021; Grigorieva et al., 2020; Zamir et al., 2020).

This study aimed to present a mathematical model for the dynamics of COVID-19 spread among human population. The constructed model was applied on the data obtained from three regions (Americas, Europe and southeast Asia) for the period between 1st May 2021 and 31st July 2021. Based on the above-mentioned literature, no one considered the fractional order analysis of COVID-19 model by considering such type of compartmental study such as by including quarantine and hospitalization or asymptomatic pre-symptomatic or symptomatic classes which makes it a more general model. Moreover, in the present analysis, we have considered the recent time interval in order to choose the real reported data which can give us the most accurate future scenario of the disease. Introduction and detailed literature review is provided in Section 1 of this manuscript while the basic preliminaries are given Section 2. The mathematical formulation of the considered problem is provided is Section 3. Positivity and boundedness of the considered model and the equilibria and basic reproduction number was also calculated which are given in Sections 4 and 5 respectively. Moreover, the classical model was generalized using Atangana-Baleanu fractional operator which has nonlocal kernel and is provided in Section 6. The uniqueness for the solution fractional model is also shown and is given in Section 7. The graphical solutions of the considered model were achieved via numerical scheme by making use of computational software MATLAB which is provided in Section 8. The model fitting of the considered problem is given in Section 9 while the discussion and conclusion of the results are elaborated in Sections 10 and 11 respectively. On the basis of available data, the future scenario for the spread of COVID-19 was predicted for

the next 200 days. The effect of fractional parameter ϕ was shown graphically. The impact of quarantine and hospitalization on the dynamics of COVID-19 among different classes was dementated.

2. Basic Preliminaries

Definition 2.1. The Atangana-Baleanu (AB) time fractional derivative in Caputo sense with fractional order ϕ is defined as (Atangana and Baleanu, 2016; Atangana and İğret Araz, 2021).

$$ {}^{ABC}_{a}\wp^{\phi}_{t} g(t) = \frac{G(\phi)}{1-\phi}\int_a^t E_\phi\left(\frac{-\phi(t-\xi)^{\phi}}{1-\phi}\right) g^{'}(\xi)d\xi, \quad \text{for} \quad 0<\phi<1. \tag{1} $$

Here, $G(\phi)$ is the normalization function and $E_\phi(.)$ is the Mittage-Leffler function (Sene, 2020).

Definition 2.2. The integral operator for the ABC fractional derivative can be defined as (Atangana, 2017; Atangana and İğret Araz, 2021):

$$ {}^{ABC}_{a}I^{\phi}_{t} g(t) = \frac{1-\phi}{G(\phi)}g(t) + \frac{\phi}{G(\phi)\Gamma(\phi)}\int_a^t (t-\xi)^{\phi-1} g(\xi)d\xi. \tag{2} $$

Definition 2.3. The numerical scheme for the solution of fractional order ODE is defined by Toufik and Atangana (Toufik and Atangana, 2017):

Consider a non-linear fractional ODE:

$$ {}^{ABC}\wp^{\phi}_{t} g(t) = w(t, g(t)) \text{with} g(0) = g_0 \tag{3} $$

The numerical solution for Eq. (3) is given as (Toufik and Atangana, 2017):

$$ g_{z+1} = g_0 + \frac{1-\phi}{G(\phi)}w(t_z, g(t_z)) + \frac{\phi}{G(\phi)}\sum_{r=0}^{z}\Big[\frac{d^{\phi}w(t_r, g(t_r))}{\Gamma(\phi+2)}\Big\{(z+1-r)^{\phi}(z+2-r+\phi) - (z-r)^{\phi}(z+2-r+2\phi)\Big\} $$

$$ -\frac{d^{\phi}w(t_{r-1}, g(t_{r-1}))}{\Gamma(\phi+2)}\Big\{(z+1-r)^{\phi+1} - (z-r)^{\phi}(z+1-r+\phi)\Big\}\Big]. \tag{4} $$

3. Mathematical Modeling

In the present model, we have considered the spread of COVID-19 in the human population in different continents of the world i.e., southeast Asia, Europe and Americas (North and South America). The total population is denoted with $N(t)$ which is further classified into different compartments i.e., susceptible population is denoted by $S(t)$, $E(t)$ are the exposed, pre-symptomatic are denoted with $A_P(t)$, while symptomatic and asymptomatic individuals are represented by $A(t)$ and $I(t)$respectively. Similarly, $Q(t)$ and $H(t)$ are the quarantined and recovered infectious individuals and $R(t)$ are the recovered or removed/deceased individuals. The flow diagram for the considered problem is displayed in Fig. 1, where susceptible individuals can interact with $A_P(t), A(t), I(t), Q(t)$ and $H(t)$ with a route $(\mu_A A + \mu_{A_P}A_P + \mu_I I + \mu_Q Q + \mu_H H)\frac{S}{N}$ and become exposed. More importantly, $E(t)$ consists of early-infected individuals. Similarly, the exposed individuals further enter to the pre-symptomatic compartment with a rate of σ whereas the pre-symptomatic $A_P(t)$ has the ability to transmit the disease. After the completion of mean incubation period, the individuals are divided in to two groups. Some of the infectious individuals have the disease symptoms while some are not. The individuals which do not have clear symptoms will enter to the asymptomatic class $A(t)$ with a rate of $(1-\zeta)\psi_A$ while those individuals having clear clinical symptoms of COVID-19 will enter to the symptomatic class $I(t)$ with the positive rates $\zeta\psi_I$. Similarly, some of the pre-symptomatic class will recover or die out due to the infection with the positive rate ψ_R while some of the pre-symptomatic individuals will enter to the quarantine class with a positive rate ψ_Q. Additionally, the symptomatic infectious individuals are quarantined or hospitalized with a positive rate κ_Q and κ_H respectively. κ_R and λ_R are the recovery or removal rates due to the disease of symptomatic or asymptomatic infected individuals respectively. At the last, these hospitalized and quarantined individuals are recovered or removed due to the disease with the rates η_R and β_R respectively. The natural death rate of all the classes is denoted with δ while the recruitment or birth rate is denoted by Λ. The flow diagram of the considered model for the spread of COVID-19 is given as:

The system of equations for the considered problem with non-negative IC's is given by:

$$ \begin{cases} \frac{dS}{dt} = \Lambda - \left(\mu_A A + \mu_{A_P}A_P + \mu_I I + \mu_Q Q + \mu_H H\right)\frac{S}{N} - \delta S, \\ \frac{dE}{dt} = \left(\mu_A A + \mu_{A_P}A_P + \mu_I I + \mu_Q Q + \mu_H H\right)\frac{S}{N} - E(\sigma+\delta), \\ \frac{dA_P}{dt} = \sigma E - ((1-\zeta)\psi_A + \zeta\psi_I + \psi_R + \psi_Q + \delta)A_P, \\ \frac{dA}{dt} = (1-\zeta)\psi_A A_P - (\lambda_R + \delta)A, \\ \frac{dI}{dt} = \zeta\psi_I A_P - (\kappa_Q + \kappa_H + \kappa_R + \delta)I, \\ \frac{dQ}{dt} = \psi_Q A_P + \kappa_Q I - (\beta_R + \delta)Q, \\ \frac{dH}{dt} = \kappa_H I - (\eta_R + \delta)H, \\ \frac{dR}{dt} = \lambda_R A + \psi_R A_P + \kappa_R I + \eta_R H + \beta_R Q - \delta R. \end{cases} \tag{5} $$

With

$$ \begin{cases} S(0) = S_0 \geq 0, \;\; E(0) = E_0 \geq 0, \;\; A_P(0) = A_{P_0} * \geq 0, \;\; A(0) = A_0 \geq 0, \\ I(0) = I_0 \geq 0, \;\; Q(0) = Q_0 \geq 0, \;\; H(0) = H_0 \geq 0, \;\; R(0) = R_0 \geq 0. \end{cases} \tag{6} $$

4. Positivity and Boundedness of the COVID-19 Model

In this section, we will show that the solution of the considered problem is bounded as well as non-negative. For this, we will state the following lemma (AHMAD et al., 2021; AHMAD et al., 2021; AHMAD et al., 2021; AHMAD et al., 2021; Z. Ahmad et al., 2020b, 2020a):

Lemma 4.1. *Consider* $\Phi \subset \mathbb{R}\times\mathbb{C}^n$ *is open,* $g_q \in \mathbb{C}(\Phi, \mathbb{R}), q = 1, 2, ., n$. If $g_q\big|_{y_q(t)=0, Y_t\in\mathbb{C}} + 0^n \geq 0$, $Y_t = (y_{1t}, y_{2t}, ., y_{nt})^T$, $q = 1, 2, ., n$, then $\mathbb{C}^n_{+0}\{\varphi = (\varphi_1, \varphi_2, ., \varphi_n) : \varphi \in \mathbb{C}([-v, 0], \mathbb{R}^n_{+0})\}$ is the invariant domain of the subsequent equations.

$$ \frac{dy_q(t)}{dt} = g_q(t, Y_t), t \geq \rho, q = 1, 2, ., n. \tag{7} $$

Where

$$\mathbb{R}^{n}_{+0}\{(y_1, y_2, ., y_n) : y_q \geq 0, \quad q = 1, 2, ., n\} \tag{8}$$

Preposition 4.1. *The system* (5) *is invariant in* $\mathbb{R}^{8}_{+}$.

Proof: By rewriting the system (5), we have:

$$\frac{dW}{dt} = M(W(t)), W(0) = W_0 \geq 0, \tag{9}$$

$$M(W(t)) = \begin{pmatrix} M_1(W), M_2(W), M_3(W), M_4(W), \\ M_5(W), M_6(W), M_7(W), M_8(W) \end{pmatrix}^{T}. \tag{10}$$

We noted that

$$\begin{cases} \left.\frac{dS}{dt}\right|_{S=0} = \Lambda \geq 0, \\ \left.\frac{dE}{dt}\right|_{E=0} = (\mu_A A + \mu_{A_P} A_P + \mu_I I + \mu_Q Q + \mu_H H)\frac{S}{(S+A+A_P+I+Q+H+R+D)} \geq 0, \\ \left.\frac{dA_P}{dt}\right|_{A_P=0} = \sigma E \geq 0, \\ \left.\frac{dA}{dt}\right|_{A=0} = (1-\zeta)\psi_A A_P \geq 0, \\ \left.\frac{dI}{dt}\right|_{I=0} = \zeta\psi_I A_P \geq 0, \\ \left.\frac{dQ}{dt}\right|_{Q=0} = \psi_Q A_P + \kappa_Q I \geq 0, \\ \left.\frac{dH}{dt}\right|_{H=0} = \kappa_H I \geq 0, \\ \left.\frac{dR}{dt}\right|_{R=0} = \lambda_R A + \psi_R A_P + \kappa_R I + \eta_R H + \beta_R Q \geq 0. \end{cases} \tag{11}$$

Hence, $\mathbb{R}^{8}_{+}$ is invariant set.

Preposition 4.2. *The system* (5) *is bounded in the region:*

$$\Phi = \left\{(S(t), E(t), A_P(t), A(t), I(t), Q(t), H(t), R(t)) \in \mathbb{R}^8 : N(t) \leq \frac{\Lambda}{\delta}\right\}.$$

Proof:. Boundedness of the problem (5) can be verified by adding all equations of system (5), we obtained:

$$\frac{dN(t)}{dt} = \Lambda - \delta N, \text{with} N(0) - N_0 \geq 0. \tag{12}$$

The solution of Eq. (12) takes the form:

$$N(t) \leq N_0 e^{-\delta t} + \frac{\Lambda}{\delta}(1 - e^{-\delta t}). \tag{13}$$

It can be clearly seen from Eq. (13) that if $t \to \infty$ then $N(t) \leq \frac{\Lambda}{\delta}$ which means that the feasible region for the given model will be:

$$\Phi = \left\{(S(t), E(t), A_P(t), A(t), I(t), Q(t), H(t), R(t)) \in \mathbb{R}^8 : N(t) \leq \frac{\Lambda}{\delta}\right\}. \tag{14}$$

Hence the solution of the considered COVID-19 model is bounded.

5. Model Equilibria and Basic Reproduction Number

The possible equilibrium points of model (5) can be obtained via the steady state by assuming:

$$\left\{\frac{dS}{dt} = \frac{dE}{dt} = \frac{dA_P}{dt} = \frac{dA}{dt} = \frac{dI}{dt} = \frac{dQ}{dt} = \frac{dH}{dt} = \frac{dR}{dt} = 0\right. \tag{15}$$

Using Eq. (15), model (5) becomes:

$$\begin{cases} 0 = \lambda - \left(\mu_E E + \mu_A A + \mu_{A_P} A_P + \mu_I I + \mu_Q Q + \mu_H H\right)\frac{S}{N} - \delta S, \\ 0 = \left(\mu_A A + \mu_{A_P} A_P + \mu_I I + \mu_Q Q + \mu_H H\right)\frac{S}{N} - \sigma E - \delta E, \\ 0 = \sigma E - ((1-\zeta)\psi_A + \zeta\psi_I + \psi_R + \psi_D + \psi_Q + \delta)A_P, \\ 0 = (1-\zeta)\psi_A A_P - (\lambda_R + \lambda_D + \delta)A, \\ 0 = \zeta\psi_I A_P - (\kappa_Q + \kappa_H + \kappa_R + \kappa_D + \delta)I, \\ 0 = \psi_Q A_P + \kappa_Q I - (\beta_R Q + \beta_D Q + \delta)Q, \\ 0 = \kappa_H I - (\eta_R + \eta_D + \delta)H, \\ 0 = \lambda_R A + \psi_R A_P + \kappa_R I + \eta_R H + \beta_R Q - \delta R. \end{cases} \tag{16}$$

The possible unique disease-free equilibrium (DFE) of system (16) can be achieved by considering $E = A_P = A = I = Q = H = R = 0$. The possible DFE is given as:

$$\Psi_{DFE} = (S^0, E^0, A_P^0, A^0, I^0, Q^0, H^0, R^0) = \left(\frac{\Lambda}{\delta}, 0, 0, 0, 0, 0, 0, 0\right). \tag{17}$$

Now have to compute the basic reproduction number $\Re_0$. The basic reproduction number $\Re_0$ gives the average number of the secondary infections created by a single infective individual during its entire infection period in a susceptible individuals (Khajanchi et al., 2021a). $\Re_0$ is typically known as a basic reproduction number or a contact number in the epidemiological models [1,17] and obtained by next generation matrix approach (Van Den Driessche and Watmough, 2002a). For this, we introduce the two matrices F and V at Ψ_{DFE} by applying the procedure of Next Generation Technique (Van Den Driessche and Watmough, 2002b):

$$F = \begin{bmatrix} 0 & \mu_{A_P} & \mu_A & \mu_I & \mu_Q & \mu_H \\ 0 & 0 & 0 & 0 & 0 & 0 \\ 0 & 0 & 0 & 0 & 0 & 0 \\ 0 & 0 & 0 & 0 & 0 & 0 \\ 0 & 0 & 0 & 0 & 0 & 0 \\ 0 & 0 & 0 & 0 & 0 & 0 \end{bmatrix} \tag{18}$$

and

$$V = \begin{bmatrix} (\sigma+\delta) & 0 & 0 & 0 & 0 & 0 \\ -\sigma & ((1-\zeta)\psi_A + \zeta\psi_I + \psi_R + \psi_Q + \delta) & 0 & 0 & 0 & 0 \\ 0 & -(1-\zeta)\psi_A & \lambda_R + \delta & 0 & 0 & 0 \\ 0 & -\zeta\psi_I & 0 & (\kappa_Q + \kappa_H + \kappa_R + \delta) & 0 & 0 \\ 0 & -\psi_Q & 0 & -\kappa_Q & \beta_R + \delta & 0 \\ 0 & 0 & 0 & -\kappa_H & 0 & \eta_R + \delta \end{bmatrix} \tag{19}$$

According to the next generation technique given in (Van Den Driessche and Watmough, 2002b) [28], the spectral radius $\rho(FV^{-1})$ is the essential $\Re_0$ which is given below:

$$\Re_0 = \frac{(\mu_A\vartheta_4 + \vartheta_3\mu_{A_P})\sigma}{\vartheta_1\vartheta_2\vartheta_3} + \frac{\zeta\sigma\psi_I(\kappa_H + \vartheta_7\mu_I)}{\vartheta_1\vartheta_2\vartheta_5\vartheta_7} + \frac{(\zeta\kappa_Q\psi_I + \vartheta_5\psi_Q)\sigma\mu_Q}{\vartheta_1\vartheta_2\vartheta_5\vartheta_6}, \tag{20}$$

Where

$$\vartheta_1 = (1-\zeta)\psi_A + \zeta\psi_I + \psi_R + \psi_Q + \delta,\ \ \vartheta_2 = \sigma + \delta,\ \ \vartheta_3 = \lambda_R + \delta,$$
$$\vartheta_4 = (1-\zeta)\psi_A,\ \ \vartheta_5 = \kappa_Q + \kappa_H + \kappa_R + \delta,\ \ \vartheta_6 = \beta_R + \delta,\ \ \vartheta_7 = \eta_R + \delta. \tag{21}$$

Next, we have to find the endemic equilibrium (EE) of the considered problem which is symbolized by $\Psi_{EE} = (S^*, E^*, A_P^*, A^*, I^*, Q^*, H^*, R^*)$ and is given as:

$$\begin{cases} S^* = \dfrac{\Lambda}{\delta+\chi},\ E^* = \dfrac{\chi S^*}{\sigma+\delta},\ A_P^* = \dfrac{E^*\sigma}{\vartheta_1},\ A^* = \dfrac{A_P^*\vartheta_4}{\lambda_R+\delta}, \\ I^* = \dfrac{\zeta\psi_I A_P^*}{\kappa_Q+\kappa_H+\kappa_R+\delta},\ Q^* = \dfrac{A_P^*(\zeta\kappa_Q\psi_I+\vartheta_5\psi_Q)}{\vartheta_5\vartheta_6},\ H^* = \dfrac{I^*\kappa_H}{\kappa_Q+\kappa_H+\kappa_R+\delta}, \\ R^* = \dfrac{A^*\lambda_R}{\vartheta_7\delta} + \dfrac{H^*\eta_R}{\vartheta_5\vartheta_7\delta} + \dfrac{I^*\beta_R\kappa_Q}{\vartheta_6\delta} + \dfrac{I^*\kappa_R}{\delta} + \dfrac{A_P^*\beta_R\psi_Q}{\vartheta_6\delta} + \dfrac{\psi_R}{\vartheta_1\vartheta_2\delta(\delta+\chi)}. \end{cases} \tag{22}$$

Where

$$\chi^* = \frac{\mu_A A^* + \mu_{A_P}A_P^* + \mu_I I^* + \mu_Q Q^* + \mu_H H^*}{N^*}.$$

6. Fractional Model of COVID-19 with Mittag-Leffler Function

To generalize the classical model of COVID-19 given in Eq. (5), we apply the definition of Atangana-Baleanu fractional operator in Caputo sense. Thus, Eq. (5) becomes:

$$\begin{cases} {}^{ABC}\wp_t^\phi S(t) = \lambda - \left(\mu_A A + \mu_{A_P}A_P + \mu_I I + \mu_Q Q + \mu_H H\right)\dfrac{S}{N} - \delta S, \\ {}^{ABC}\wp_t^\phi E(t) = \left(\mu_A A + \mu_{A_P}A_P + \mu_I I + \mu_Q Q + \mu_H H\right)\dfrac{S}{N} - (E+\delta)E, \\ {}^{ABC}\wp_t^\phi A_P(t) = \sigma E - ((1-\zeta)\psi_A + \zeta\psi_I + \psi_R + \psi_Q + \delta)A_P, \\ {}^{ABC}\wp_t^\phi A(t) = (1-\zeta)\psi_A A_P - (\lambda_R+\delta)A, \\ {}^{ABC}\wp_t^\phi I(t) = \zeta\psi_I A_P - (\kappa_Q+\kappa_H+\kappa_R+\delta)I, \\ {}^{ABC}\wp_t^\phi Q(t) = \psi_Q A_P + \kappa_Q I - (\beta_R+\delta)Q, \\ {}^{ABC}\wp_t^\phi H(t) = \kappa_H I - (\eta_R+\delta)H, \\ {}^{ABC}\wp_t^\phi R(t) = \lambda_R A + \psi_R A_P + \kappa_R I + \eta_R H + \beta_R Q - \delta R. \end{cases} \tag{23}$$

Where ${}^{ABC}\wp_t^\phi(.)$ is the definition of ABC fractional derivative having fractional order ϕ.

7. Uniqueness of the AB-Time Fractional Model

This section of the present paper provides the existence of a unique solution of the ABC-time fractional model, which is given in Eq. (23). Let us consider $B(\omega)$ be a Banach space of the real-valued continuous functions with supremum norm defined on the interval $\omega = [0, T]$ and $\mathfrak{F} = B(\omega)\times B(\omega)\times B(\omega)\times B(\omega)\times B(\omega)\times B(\omega)\times B(\omega)\times B(\omega)$ with the norm $\|(S,E,A_p,A,I,Q,H,R)\| = \|S\| + \|E\| + \|A_p\| + \|A\| + \|I\| + \|Q\| + \|H\| + \|R\|$, where $\|S\| = \sup\{|S(t)| : t \in \omega\}$, $\|E\| = \sup\{|E(t)| : t \in \omega\}$, $\|A_p\| = \sup\{|A_p(t)| : t \in \omega\}$, $\|A\| = \sup\{|A(t)| : t \in \omega\}$, $\|I\| = \sup\{|I(t)| : t \in \omega\}$, $\|Q\| = \sup\{|Q(t)| : t \in \omega\}$, $\|H\| = \sup\{|H(t)| : t \in \omega\}$ and $\|R\| = \sup\{|R(t)| : t \in \omega\}$. By applying the ABC-fractional integral operator given in Eq. (23), the equation takes the following form:

$$\begin{cases} S(t) - S(0) = {}_0^{ABC}I_t^\phi\left(\lambda - \left(\mu_A A + \mu_{A_P}A_P + \mu_I I + \mu_Q Q + \mu_H H\right)\dfrac{S}{N} - \delta S\right), \\ E(t) - E(0) = {}_0^{ABC}I_t^\phi\left(\left(\mu_A A + \mu_{A_P}A_P + \mu_I I + \mu_Q Q + \mu_H H\right)\dfrac{S}{N} - (E+\delta)E\right), \\ A_P(t) - A_P(0) = {}_0^{ABC}I_t^\phi(\sigma E - ((1-\zeta)\psi_A + \zeta\psi_I + \psi_R + \psi_Q + \delta)A_P), \\ A(t) - A(0) = {}_0^{ABC}I_t^\phi((1-\zeta)\psi_A A_P - (\lambda_R+\delta)A), \\ I(t) - I(0) = {}_0^{ABC}I_t^\phi(\zeta\psi_I A_P - (\kappa_Q+\kappa_H+\kappa_R+\delta)I), \\ Q(t) - Q(0) = {}_0^{ABC}I_t^\phi(\psi_Q A_P + \kappa_Q I - (\beta_R+\delta)Q), \\ H(t) - H(0) = {}_0^{ABC}I_t^\phi(\kappa_H I - (\eta_R+\delta)H), \\ R(t) - R(0) = {}_0^{ABC}I_t^\phi(\lambda_R A + \psi_R A_P + \kappa_R I + \eta_R H + \beta_R Q - \delta R). \end{cases} \tag{24}$$

Which implies:

$$\begin{cases} S(t) - S(0) = \dfrac{1-\phi}{G(\phi)}H(t,S(t)) + \dfrac{\phi}{G(\phi)\Gamma(\phi)}\displaystyle\int_0^t H(\xi,S(\xi))(t-\xi)^{\phi-1}d\xi, \\ E(t) - E(0) = \dfrac{1-\phi}{G(\phi)}H(t,E(t)) + \dfrac{\phi}{G(\phi)\Gamma(\phi)}\displaystyle\int_0^t H(\xi,E(\xi))(t-\xi)^{\phi-1}d\xi, \\ A_P(t) - A_P(0) = \dfrac{1-\phi}{G(\phi)}H(t,A_P(t)) + \dfrac{\phi}{G(\phi)\Gamma(\phi)}\displaystyle\int_0^t H(\xi,A_P(\xi))(t-\xi)^{\phi-1}d\xi, \\ A(t) - A(0) = \dfrac{1-\phi}{G(\phi)}H(t,A(t)) + \dfrac{\phi}{G(\phi)\Gamma(\phi)}\displaystyle\int_0^t H(\xi,A(\xi))(t-\xi)^{\phi-1}d\xi, \\ I(t) - I(0) = \dfrac{1-\phi}{G(\phi)}H(t,I(t)) + \dfrac{\phi}{G(\phi)\Gamma(\phi)}\displaystyle\int_0^t H(\xi,I(\xi))(t-\xi)^{\phi-1}d\xi, \\ Q(t) - Q(0) = \dfrac{1-\phi}{G(\phi)}H(t,Q(t)) + \dfrac{\phi}{G(\phi)\Gamma(\phi)}\displaystyle\int_0^t H(\xi,Q(\xi))(t-\xi)^{\phi-1}d\xi, \\ H(t) - H(0) = \dfrac{1-\phi}{G(\phi)}H(t,H(t)) + \dfrac{\phi}{G(\phi)\Gamma(\phi)}\displaystyle\int_0^t H(\xi,H(\xi))(t-\xi)^{\phi-1}d\xi, \\ R(t) - R(0) = \dfrac{1-\phi}{G(\phi)}H(t,R(t)) + \dfrac{\phi}{G(\phi)\Gamma(\phi)}\displaystyle\int_0^t H(\xi,R(\xi))(t-\xi)^{\phi-1}d\xi. \end{cases} \tag{25}$$

Where

$$\begin{cases} H(t,S(t)) = \lambda - \left(\mu_A A + \mu_{A_P}A_P + \mu_I I + \mu_Q Q + \mu_H H\right)\dfrac{S}{N} - \delta S, \\ H(t,E(t)) = \left(\mu_A A + \mu_{A_P}A_P + \mu_I I + \mu_Q Q + \mu_H H\right)\dfrac{S}{N} - (E+\delta)E, \\ H(t,A_P(t)) = \sigma E - ((1-\zeta)\psi_A + \zeta\psi_I + \psi_R + \psi_Q + \delta)A_P, \\ H(t,A(t)) = (1-\zeta)\psi_A A_P - (\lambda_R+\delta)A, \\ H(t,I(t)) = \zeta\psi_I A_P - (\kappa_Q+\kappa_H+\kappa_R+\delta)I, \\ H(t,Q(t)) = \psi_Q A_P + \kappa_Q I - (\beta_R+\delta)Q, \\ H(t,H(t)) = \kappa_H I - (\eta_R+\delta)H, \\ H(t,R(t)) = \lambda_R A + \psi_R A_P + \kappa_R I + \eta_R H + \beta_R Q - \delta R. \end{cases} \tag{26}$$

The expressions $H(t,S(t))$, $H(t,E(t))$, $H(t,A_P(t))$, $H(t,A(t))$, $H(t,I(t))$, $H(t,Q(t))$, $H(t,H(t))$ and $H(t,R(t))$ are thought to satisfy the Lipchitz condition if and only if $S(t), E(t), A_P(t), A(t), I(t), Q(t), H(t)$ and $R(t)$ are upper bounded. Let us consider $S(t)$ and $S_1(t)$ be the two functions, then we have:

$$\|\varsigma(t,S(t)) - \varsigma(t,S_1(t))\| = \left\| \begin{matrix} -\lambda^\beta S(t)E(t) + \left(\kappa^\beta - \sigma^\beta S(t)\right)C_1(t) + \psi^\beta C_2(t) \\ +\lambda^\beta S_1(t)E(t) - \left(\kappa^\beta - \sigma^\beta S_1(t)\right)C_1(t) - \psi^\beta C_2(t) \end{matrix} \right\| \tag{27}$$

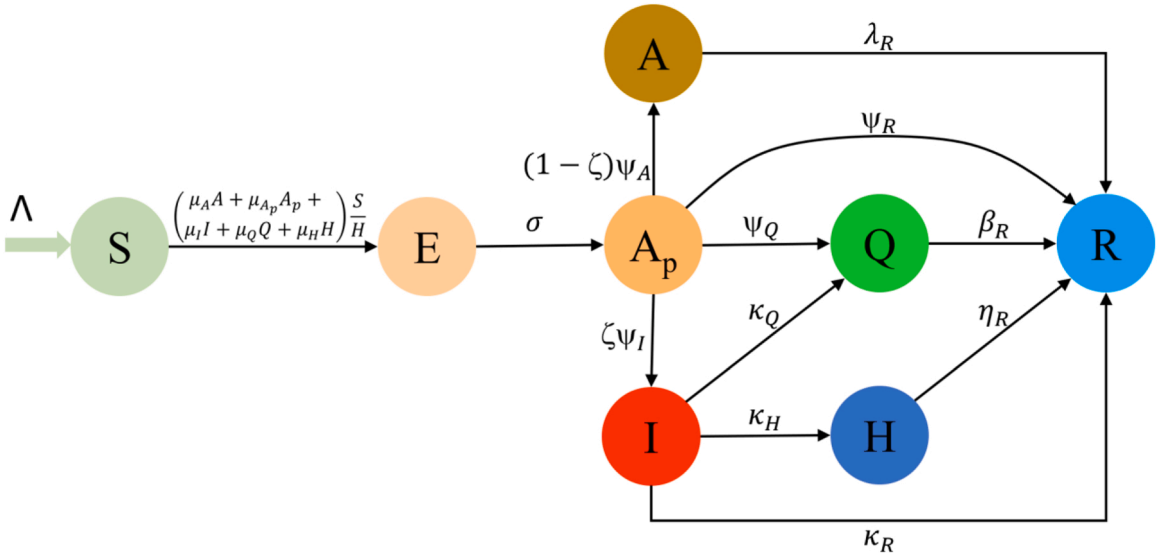

Fig. 1. Graphical Scheme of the model.

$$\|H(t,S(t))-H(t,S_1(t))\|=\left\|\begin{matrix}\lambda-\left(\mu_A A+\mu_{A_P}A_P+\mu_I I+\mu_Q Q+\mu_H H\right)\frac{S}{N}-\delta S\\ -\lambda+\left(\mu_A A+\mu_{A_P}A_P+\mu_I I+\mu_Q Q+\mu_H H\right)\frac{S_1}{N}+\delta S_1\end{matrix}\right\| \tag{28}$$

Equivalent to:

$$\|H(t,S(t))-H(t,S_1(t))\|\le L_1\|S(t)-S_1(t)\| \tag{29}$$

Where $L_1=\left\|\left(\mu_A A+\mu_{A_P}A_P+\mu_I I+\mu_Q Q+\mu_H H\right)\left(\frac{S}{N}-\frac{S_1}{N_1}\right)+\delta(S_1-S)\right\|$ having $N_1=S_1+E+A_P+A+I+Q+H+R$ is the corresponding Lipchitz constant.

In similar way, we can attain:

$$\begin{cases}\|H(t,E(t))-H(t,E_1(t))\|\le L_2\|E(t)-E_1(t)\|,\\ \left\|H(t,A_P(t))-H\left(t,A_{P,1}(t)\right)\right\|\le L_3\left\|A_P(t)-A_{P,1}(t)\right\|,\\ \|H(t,A(t))-H(t,A_1(t))\|\le L_4\|A(t)-A_1(t)\|,\\ \|H(t,I(t))-H(t,I_1(t))\|\le L_5\|I(t)-I_1(t)\|,\\ \|H(t,Q(t))-H(t,Q_1(t))\|\le L_6\|Q(t)-Q_1(t)\|,\\ \|H(t,H(t))-H(t,H_1(t))\|\le L_7\|H(t)-H_1(t)\|,\\ \|H(t,R(t))-H(t,R_1(t))\|\le L_8\|R(t)-R_1(t)\|.\end{cases} \tag{30}$$

Hence, the above functions satisfy the Lipchitz condition with the corresponding Lipchitz constants, i.e., $L_1, L_2, L_3, L_4, L_5, L_6, L_7$ and L_8.

Recursively, we can write Eq. (25) as:

$$\begin{cases}S_m(t)-S(0)=\frac{1-\phi}{G(\phi)}H(t,S_{m-1}(t))+\frac{\phi}{G(\phi)\Gamma(\phi)}\int_0^t H(\xi,S_{m-1}(\xi))(t-\xi)^{\phi-1}d\xi,\\ E_m(t)-E(0)=\frac{1-\phi}{G(\phi)}H(t,E_{m-1}(t))+\frac{\phi}{G(\phi)\Gamma(\phi)}\int_0^t H(\xi,E_{m-1}(\xi))(t-\xi)^{\phi-1}d\xi,\\ A_{P,m}(t)-A_{P,m-1}(0)=\frac{1-\phi}{G(\phi)}H\left(t,A_{P,m-1}(t)\right)+\frac{\phi}{G(\phi)\Gamma(\phi)}\int_0^t H\left(\xi,A_{P,m-1}(\xi)\right)(t-\xi)^{\phi-1}d\xi,\\ A_m(t)-A(0)=\frac{1-\phi}{G(\phi)}H(t,A_{m-1}(t))+\frac{\phi}{G(\phi)\Gamma(\phi)}\int_0^t H(\xi,A_{m-1}(\xi))(t-\xi)^{\phi-1}d\xi,\\ I_m(t)-I(0)=\frac{1-\phi}{G(\phi)}H(t,I_{m-1}(t))+\frac{\phi}{G(\phi)\Gamma(\phi)}\int_0^t H(\xi,I_{m-1}(\xi))(t-\xi)^{\phi-1}d\xi,\\ Q_m(t)-Q(0)=\frac{1-\phi}{G(\phi)}H(t,Q_{m-1}(t))+\frac{\phi}{G(\phi)\Gamma(\phi)}\int_0^t H(\xi,Q_{m-1}(\xi))(t-\xi)^{\phi-1}d\xi,\\ H_m(t)-H(0)=\frac{1-\phi}{G(\phi)}H(t,H_{m-1}(t))+\frac{\phi}{G(\phi)\Gamma(\phi)}\int_0^t H(\xi,H_{m-1}(\xi))(t-\xi)^{\phi-1}d\xi,\\ R_m(t)-R(0)=\frac{1-\phi}{G(\phi)}H(t,R_{m-1}(t))+\frac{\phi}{G(\phi)\Gamma(\phi)}\int_0^t H(\xi,R_{m-1}(\xi))(t-\xi)^{\phi-1}d\xi.\end{cases} \tag{31}$$

By the difference of consecutive terms, we get:

$$\begin{cases}
\coprod_{S,m}(t) = S_m(t) - S_{m-1}(t) = \dfrac{1}{G(\phi)}\left(\begin{array}{l}(1-\phi)\{H(t,S_{m-1}(t)) - H(t,S_{m-2}(t))\} \\ +\dfrac{\phi}{\Gamma(\phi)}\displaystyle\int_0^t \{H(\xi,S_{m-1}(\xi)) - H(\xi,S_{m-2}(\xi))\}(t-\xi)^{\phi-1}d\xi\end{array}\right), \\
\coprod_{E,m}(t) = E_m(t) - E_{m-1}(t) = \dfrac{1}{G(\phi)}\left(\begin{array}{l}(1-\phi)\{H(t,E_{m-1}(t)) - H(t,E_{m-2}(t))\} \\ +\dfrac{\phi}{\Gamma(\phi)}\displaystyle\int_0^t \{H(\xi,E_{m-1}(\xi)) - H(\xi,E_{m-2}(\xi))\}(t-\xi)^{\phi-1}d\xi\end{array}\right), \\
\coprod_{A_P,m}(t) = A_{P,m}(t) - A_{P,m-1}(t) = \dfrac{1}{G(\phi)}\left(\begin{array}{l}(1-\phi)\{H(t,A_{P,m-1}(t)) - H(t,A_{P,m-2}(t))\} \\ +\dfrac{\phi}{\Gamma(\phi)}\displaystyle\int_0^t \{H(\xi,A_{P,m-1}(\xi)) - H(\xi,A_{P,m-2}(\xi))\}(t-\xi)^{\phi-1}d\xi\end{array}\right), \\
\coprod_{A,m}(t) = A_m(t) - A_{m-1}(t) = \dfrac{1}{G(\phi)}\left(\begin{array}{l}(1-\phi)\{H(t,A_{m-1}(t)) - H(t,A_{m-2}(t))\} \\ +\dfrac{\phi}{\Gamma(\phi)}\displaystyle\int_0^t \{H(\xi,A_{m-1}(\xi)) - H(\xi,A_{m-2}(\xi))\}(t-\xi)^{\phi-1}d\xi\end{array}\right), \\
\coprod_{Q,m}(t) = Q_m(t) - Q_{m-1}(t) = \dfrac{1}{G(\phi)}\left(\begin{array}{l}(1-\phi)\{H(t,Q_{m-1}(t)) - H(t,Q_{m-2}(t))\} \\ +\dfrac{\phi}{\Gamma(\phi)}\displaystyle\int_0^t \{H(\xi,Q_{m-1}(\xi)) - H(\xi,Q_{m-2}(\xi))\}(t-\xi)^{\phi-1}d\xi\end{array}\right), \\
\coprod_{H,m}(t) = H_m(t) - H_{m-1}(t) = \dfrac{1}{G(\phi)}\left(\begin{array}{l}(1-\phi)\{H(t,H_{m-1}(t)) - H(t,H_{m-2}(t))\} \\ +\dfrac{\phi}{\Gamma(\phi)}\displaystyle\int_0^t \{H(\xi,H_{m-1}(\xi)) - H(\xi,H_{m-2}(\xi))\}(t-\xi)^{\phi-1}d\xi\end{array}\right), \\
\coprod_{R,m}(t) = R_m(t) - R_{m-1}(t) = \dfrac{1}{G(\phi)}\left(\begin{array}{l}(1-\phi)\{H(t,R_{m-1}(t)) - H(t,R_{m-2}(t))\} \\ +\dfrac{\phi}{\Gamma(\phi)}\displaystyle\int_0^t \{H(\xi,R_{m-1}(\xi)) - H(\xi,R_{m-2}(\xi))\}(t-\xi)^{\phi-1}d\xi\end{array}\right).
\end{cases} \tag{32}$$

It is important to mention here that $S_m(t) = \sum_{k=0}^{m}\coprod_{S,k}(t)$, $E_m(t) = \sum_{k=0}^{m}\coprod_{E,k}(t)$, $A_{P,m}(t) = \sum_{k=0}^{m}\coprod_{A_P,k}(t)$, $A_m(t) = \sum_{k=0}^{m}\coprod_{A,k}(t)$, $I_m(t) = \sum_{k=0}^{m}\coprod_{I,k}(t)$, $Q_m(t) = \sum_{k=0}^{m}\coprod_{Q,k}(t)$, $H_m(t) = \sum_{k=0}^{m}\coprod_{H,k}(t)$, and $R_m(t) = \sum_{k=0}^{m}\coprod_{R,k}(t)$. Moreover, using Eqs. (29) and (30) and taking $\coprod_{S,m-1}(t) = S_{m-1}(t) - S_{m-2}(t)$, $\coprod_{E,m-1}(t) = E_{m-1}(t) - E_{m-2}(t)$, $\coprod_{A_P,m-1}(t) = A_{P,m-1}(t) - A_{P,m-2}(t)$, $\coprod_{A,m-1}(t) = A_{m-1}(t) - A_{m-2}(t)$, $\coprod_{Q,m-1}(t) = Q_{m-1}(t) - Q_{m-2}(t)$, $\coprod_{H,m-1}(t) = H_{m-1}(t) - H_{m-2}(t)$ and $\coprod_{R,m-1}(t) = R_{m-1}(t) - R_{m-2}(t)$, we reach the following form:

$$\begin{cases}
\left\|\coprod_{S,m}(t)\right\| \le \dfrac{(1-\phi)}{G(\phi)}L_1\left\|\coprod_{S,m-1}(t)\right\| + \dfrac{\phi}{G(\phi)\Gamma(\phi)}\displaystyle\int_0^t L_1\left\|\coprod_{S,m-1}(\xi)\right\|(t-\xi)^{\phi-1}d\xi, \\
\left\|\coprod_{E,m}(t)\right\| \le \dfrac{(1-\phi)}{G(\phi)}L_2\left\|\coprod_{E,m-1}(t)\right\| + \dfrac{\phi}{G(\phi)\Gamma(\phi)}\displaystyle\int_0^t L_2\left\|\coprod_{E,m-1}(\xi)\right\|(t-\xi)^{\phi-1}d\xi, \\
\left\|\coprod_{A_P,m}(t)\right\| \le \dfrac{(1-\phi)}{G(\phi)}L_3\left\|\coprod_{A_P,m-1}(t)\right\| + \dfrac{\phi}{G(\phi)\Gamma(\phi)}\displaystyle\int_0^t L_3\left\|\coprod_{A_P,m-1}(\xi)\right\|(t-\xi)^{\phi-1}d\xi, \\
\left\|\coprod_{A,m}(t)\right\| \le \dfrac{(1-\phi)}{G(\phi)}L_4\left\|\coprod_{A,m-1}(t)\right\| + \dfrac{\phi}{G(\phi)\Gamma(\phi)}\displaystyle\int_0^t L_4\left\|\coprod_{A,m-1}(\xi)\right\|(t-\xi)^{\phi-1}d\xi, \\
\left\|\coprod_{I,m}(t)\right\| \le \dfrac{(1-\phi)}{G(\phi)}L_5\left\|\coprod_{I,m-1}(t)\right\| + \dfrac{\phi}{G(\phi)\Gamma(\phi)}\displaystyle\int_0^t L_5\left\|\coprod_{I,m-1}(\xi)\right\|(t-\xi)^{\phi-1}d\xi, \\
\left\|\coprod_{Q,m}(t)\right\| \le \dfrac{(1-\phi)}{G(\phi)}L_6\left\|\coprod_{Q,m-1}(t)\right\| + \dfrac{\phi}{G(\phi)\Gamma(\phi)}\displaystyle\int_0^t L_6\left\|\coprod_{Q,m-1}(\xi)\right\|(t-\xi)^{\phi-1}d\xi, \\
\left\|\coprod_{H,m}(t)\right\| \le \dfrac{(1-\phi)}{G(\phi)}L_7\left\|\coprod_{H,m-1}(t)\right\| + \dfrac{\phi}{G(\phi)\Gamma(\phi)}\displaystyle\int_0^t L_7\left\|\coprod_{H,m-1}(\xi)\right\|(t-\xi)^{\phi-1}d\xi, \\
\left\|\coprod_{R,m}(t)\right\| \le \dfrac{(1-\phi)}{G(\phi)}L_8\left\|\coprod_{R,m-1}(t)\right\| + \dfrac{\phi}{G(\phi)\Gamma(\phi)}\displaystyle\int_0^t L_8\left\|\coprod_{R,m-1}(\xi)\right\|(t-\xi)^{\phi-1}d\xi,
\end{cases} \tag{33}$$

Theorem. *The present fractional model (23) has a unique solution for* $t \in [0, T]$ *if the following condition satisfies* (AHMAD et al., 2021; AHMAD et al., 2021; AHMAD et al., 2021; AHMAD et al., 2021; Qureshi and Yusuf, 2019c; Sinan et al., 2022, 2021):

$$\frac{(1-\phi)}{G(\phi)}L_k + \frac{\phi}{G(\phi)\Gamma(\phi)}L_k b^{\phi} < 1, \quad k = 1,2,3,4,5.$$

Proof. : As it is already shown that $S(t)$, $E(t)$, $A_P(t), A(t), I(t), Q(t), H(t)$ and $R(t)$ are bounded functions. It is also shown in Eqs. (29) and (30) that $H(S(t),t)$,$H(E(t),t)$,$H(A_P(t),t)$,$H(A(t),t)$,$H(I(t),t)$,$H(Q(t),t)$,$H(H(t),t)$ and $H(R(t),t)$ satisfy the Lipchitz condition. Thus, by implementing the recursive application, Eq. (33) takes the following shape:

$$\begin{cases}
\left\|\coprod_{S,m}(t)\right\| \le \|S_0(t)\|\left(\frac{(1-\phi)}{G(\phi)}L_1 + \frac{b^{\phi}}{G(\phi)\Gamma(\phi)}L_1 b^{\phi}\right)^m, \\
\left\|\coprod_{E,m}(t)\right\| \le \|E_0(t)\|\left(\frac{(1-\phi)}{G(\phi)}L_2 + \frac{b^{\phi}}{G(\phi)\Gamma(\phi)}L_2 b^{\phi}\right)^m, \\
\left\|\coprod_{A_P,m}(t)\right\| \le \|A_{P,0}(t)\|\left(\frac{(1-\phi)}{G(\phi)}L_3 + \frac{b^{\phi}}{G(\phi)\Gamma(\phi)}L_3 b^{\phi}\right)^m, \\
\left\|\coprod_{A,m}(t)\right\| \le \|A_0(t)\|\left(\frac{(1-\phi)}{G(\phi)}L_4 + \frac{b^{\phi}}{G(\phi)\Gamma(\phi)}L_4 b^{\phi}\right)^m, \\
\left\|\coprod_{I,m}(t)\right\| \le \|I_0(t)\|\left(\frac{(1-\phi)}{G(\phi)}L_5 + \frac{b^{\phi}}{G(\phi)\Gamma(\phi)}L_5 b^{\phi}\right)^m, \\
\left\|\coprod_{Q,m}(t)\right\| \le \|Q_0(t)\|\left(\frac{(1-\phi)}{G(\phi)}L_6 + \frac{b^{\phi}}{G(\phi)\Gamma(\phi)}L_6 b^{\phi}\right)^m, \\
\left\|\coprod_{H,m}(t)\right\| \le \|H_0(t)\|\left(\frac{(1-\phi)}{G(\phi)}L_7 + \frac{b^{\phi}}{G(\phi)\Gamma(\phi)}L_7 b^{\phi}\right)^m, \\
\left\|\coprod_{R,m}(t)\right\| \le \|R_0(t)\|\left(\frac{(1-\phi)}{G(\phi)}L_8 + \frac{b^{\phi}}{G(\phi)\Gamma(\phi)}L_8 b^{\phi}\right)^m.
\end{cases} \tag{34}$$

Therefore, the above-mentioned sequences exist and satisfy $\left\|\coprod_{S,m}(t)\right\| \to 0$, $\left\|\coprod_{E,m}(t)\right\| \to 0$, $\left\|\coprod_{A_P,m}(t)\right\| \to 0$, $\left\|\coprod_{A,m}(t)\right\| \to 0$, $\left\|\coprod_{I,m}(t)\right\| \to 0$, $\left\|\coprod_{Q,m}(t)\right\| \to 0$, $\left\|\coprod_{H,m}(t)\right\| \to 0$ and $\left\|\coprod_{R,m}(t)\right\| \to 0$ as $m \to \infty$. Further, by applying the triangular inequality for any j, we get:

$$\begin{cases}
\left\|S_{m+j}(t) - S_m(t)\right\| \le \sum_{k=m+1}^{m+j} \mathfrak{F}_1^k = \frac{\mathfrak{F}_1^{m+1} - \mathfrak{F}_1^{m+j+1}}{1-\mathfrak{F}_1}, \\
\left\|E_{m+j}(t) - E_m(t)\right\| \le \sum_{k=m+1}^{m+j} \mathfrak{F}_2^k = \frac{\mathfrak{F}_2^{m+1} - \mathfrak{F}_2^{m+j+1}}{1-\mathfrak{F}_2}, \\
\left\|A_{P,m+j}(t) - A_{P,m}(t)\right\| \le \sum_{k=m+1}^{m+j} \mathfrak{F}_3^k = \frac{\mathfrak{F}_3^{m+1} - \mathfrak{F}_3^{m+j+1}}{1-\mathfrak{F}_3}, \\
\left\|A_{m+j}(t) - A_m(t)\right\| \le \sum_{k=m+1}^{m+j} \mathfrak{F}_4^k = \frac{\mathfrak{F}_4^{m+1} - \mathfrak{F}_4^{m+j+1}}{1-\mathfrak{F}_4}, \\
\left\|I_{m+j}(t) - I_m(t)\right\| \le \sum_{k=m+1}^{m+j} \mathfrak{F}_5^k = \frac{\mathfrak{F}_5^{m+1} - \mathfrak{F}_5^{m+j+1}}{1-\mathfrak{F}_5}, \\
\left\|Q_{m+j}(t) - Q_m(t)\right\| \le \sum_{k=m+1}^{m+j} \mathfrak{F}_6^k = \frac{\mathfrak{F}_6^{m+1} - \mathfrak{F}_6^{m+j+1}}{1-\mathfrak{F}_6}, \\
\left\|H_{m+j}(t) - H_m(t)\right\| \le \sum_{k=m+1}^{m+j} \mathfrak{F}_7^k = \frac{\mathfrak{F}_7^{m+1} - \mathfrak{F}_7^{m+j+1}}{1-\mathfrak{F}_7}, \\
\left\|R_{m+j}(t) - R_m(t)\right\| \le \sum_{k=m+1}^{m+j} \mathfrak{F}_8^k = \frac{\mathfrak{F}_8^{m+1} - \mathfrak{F}_8^{m+j+1}}{1-\mathfrak{F}_8},
\end{cases} \tag{35}$$

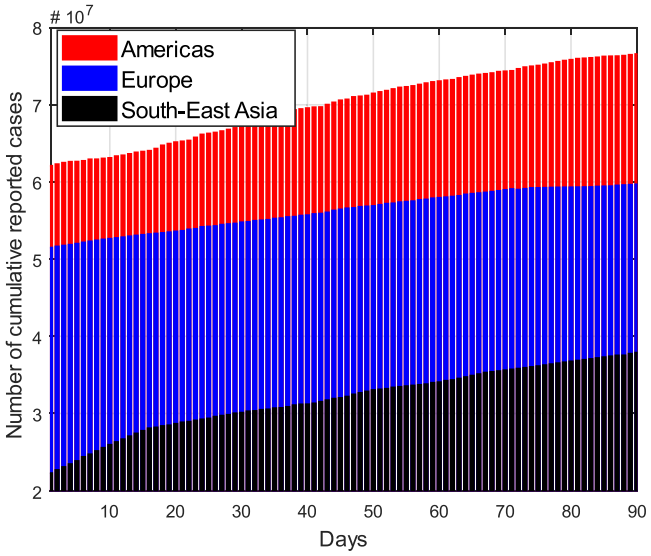

Fig. 2. Cumulative reported cases in south-east Asia, Europe and Americas between 1st May 2021 and 31st July 2021.

Table 1
List of Parameters with Description.

Parameter	Description
μ_A	Contact rate among asymptomatic and susceptible individuals
μ_{A_P}	Contact rate among pre-asymptomatic and susceptible individuals
μ_I	Contact rate among symptomatic and susceptible individuals
μ_Q	Contact rate among quarantined and susceptible individuals
μ_H	Contact rate among hospitalized and susceptible individuals
σ	Incubation period
ζ	Proportion of exposed developing asymptomatic infections
ψ_A	Disease progression rate from the pre-asymptomatic to asymptomatic individuals
ψ_I	Disease progression rate from the pre-asymptomatic to infectious individuals
ψ_Q	Quarantined rate of pre-asymptomatic individuals
κ_Q	Quarantined rate of symptomatic individuals
κ_H	Hospitalization rate of symptomatic individuals
κ_R	Recovery or removal rate of symptomatic individuals
η_R	Recovery or removal rate of hospitalized individuals
β_R	Recovery or removal rate of quarantined individuals
ψ_R	Recovery or removal rate of pre-asymptomatic individuals
λ_R	Recovery or removal rate of asymptomatic individuals
Λ	recruitment rate
δ	Natural mortality rate

Where $\frac{(1-\phi)}{G(\phi)}L_k + \frac{b^{\phi}}{G(\phi)\Gamma(\phi)}L_k < 1$ by assertion and $\mathfrak{F}_1, \mathfrak{F}_2, \mathfrak{F}_3, \mathfrak{F}_4, \mathfrak{F}_5, \mathfrak{F}_6, \mathfrak{F}_7$ are the terms and $\mathfrak{F}_8$ given enclosed in brackets of Eq. (34), correspondingly. Thus $S_m, E_m, A_{P,m}, A_m, I_m, Q_m, H_m$ and R_m represents the Cauchy sequences in $B(\varpi)$. As a result, they are all uniformly convergent. As $m \to \infty$ is applied to Eq. (31), it shows that the limit of these sequences is the model (23) unique solution. The existence of a unique solution for the system (23) is eventually established.

8. Numerical scheme for the Solution of the Fractional Model

Applying the procedure in Definition (2.3), the numerical algorithm for the model (23) can be stated as:

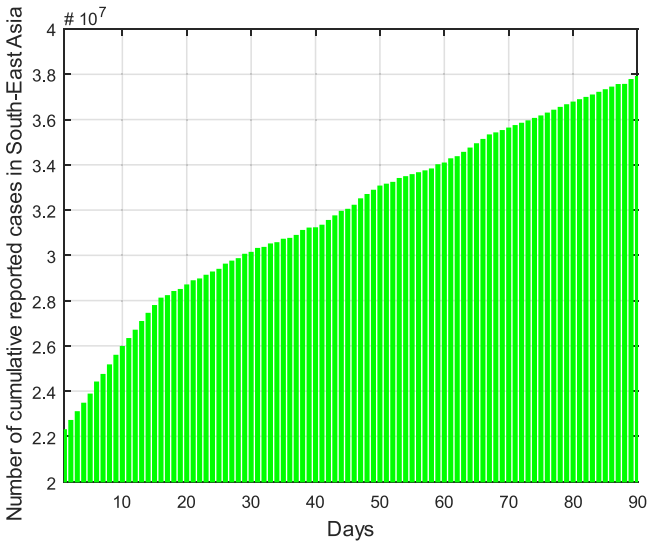

Fig. 3. Cumulative reported cases in south-east Asia between 1st May 2021 and 31st July 2021.

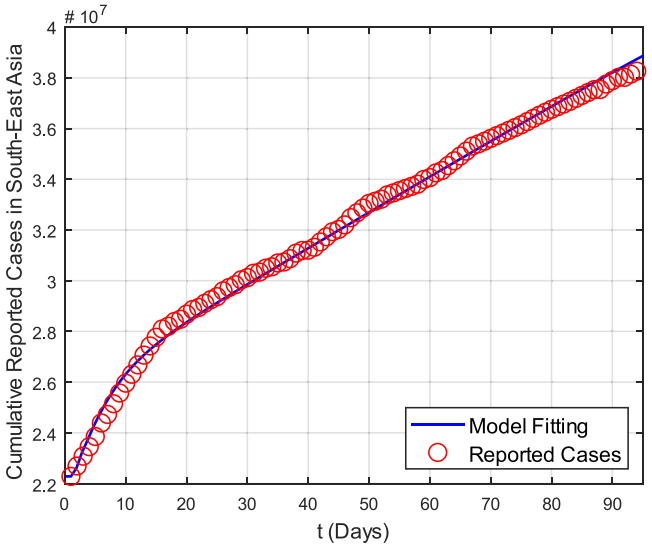

Fig. 4. Model Fitting versus reported cases in south-east Asia between 1st May 2021 and 31st July 2021.

$$\begin{cases} {}^{ABC}_{0}\mathcal{D}_t^{\phi} S(t) = H(t, S(t)), \\ {}^{ABC}_{0}\mathcal{D}_t^{\phi} E(t) = H(t, E(t)), \\ {}^{ABC}_{0}\mathcal{D}_t^{\phi} A_P(t) = H(t, A_P(t)), \\ {}^{ABC}_{0}\mathcal{D}_t^{\phi} A(t) = H(t, A(t)), \\ {}^{ABC}_{0}\mathcal{D}_t^{\phi} I(t) = H(t, I(t)), \\ {}^{ABC}_{0}\mathcal{D}_t^{\phi} Q(t) = H(t, Q(t)), \\ {}^{ABC}_{0}\mathcal{D}_t^{\phi} H(t) = H(t, H(t)), \\ {}^{ABC}_{0}\mathcal{D}_t^{\phi} R(t) = H(t, R(t)). \end{cases} \tag{36}$$

Which implies

$$S(t_{z+1}) = S(t_0) + \frac{1-\phi}{G(\phi)} H(t_z, S(t_z)) + \frac{\phi}{G(\phi)} \sum_{r=0}^{z} \left[\frac{d^{\phi} H(t_r, S(t_r))}{\Gamma(\phi+2)} \left\{ (z+1-r)^{\phi} (z+2-r+\phi) - (z-r)^{\phi} (z+2-r+2\phi) \right\} - \frac{d^{\phi} H(t_{r-1}, S(t_{r-1}))}{\Gamma(\phi+2)} \left\{ (z+1-r)^{\phi+1} - (z-r)^{\phi} (z+1-r+\phi) \right\} \right] \tag{37}$$

$$E(t_{z+1}) = E(t_0) + \frac{1-\phi}{G(\phi)} H(t_z, E(t_z)) + \frac{\phi}{G(\phi)} \sum_{r=0}^{z} \left[\frac{d^{\phi} H(t_r, E(t_r))}{\Gamma(\phi+2)} \left\{ (z+1-r)^{\phi} (z+2-r+\phi) - (z-r)^{\phi} (z+2-r+2\phi) \right\} - \frac{d^{\phi} H(t_{r-1}, E(t_{r-1}))}{\Gamma(\phi+2)} \left\{ (z+1-r)^{\phi+1} - (z-r)^{\phi} (z+1-r+\phi) \right\} \right] \tag{38}$$

$$A_P(t_{z+1}) = A_P(t_0) + \frac{1-\phi}{G(\phi)} H(t_z, A_P(t_z)) + \frac{\phi}{G(\phi)} \sum_{r=0}^{z} \left[\frac{d^{\phi} H(t_r, A_P(t_r))}{\Gamma(\phi+2)} \left\{ (z+1-r)^{\phi} (z+2-r+\phi) - (z-r)^{\phi} (z+2-r+2\phi) \right\} - \frac{d^{\phi} H(t_{r-1}, A_P(t_{r-1}))}{\Gamma(\phi+2)} \left\{ (z+1-r)^{\phi+1} - (z-r)^{\phi} (z+1-r+\phi) \right\} \right] \tag{39}$$

$$A(t_{z+1}) = A(t_0) + \frac{1-\phi}{G(\phi)}H(t_z, A(t_z)) + \\ + \frac{\phi}{G(\phi)}\sum_{r=0}^{z}\Big[\frac{d^{\phi}H(t_r, A(t_r))}{\Gamma(\phi+2)}\Big\{(z+1-r)^{\phi}(z+2-r+\phi) - (z-r)^{\phi}(z+2-r+2\phi)\Big\} - \frac{d^{\phi}H(t_{r-1}, A(t_{r-1}))}{\Gamma(\phi+2)}\Big\{(z+1-r)^{\phi+1} - (z-r)^{\phi}(z+1-r+\phi)\Big\}\Big] \tag{40}$$

$$I(t_{z+1}) = I(t_0) + \frac{1-\phi}{G(\phi)}H(t_z, I(t_z)) + \\ + \frac{\phi}{G(\phi)}\sum_{r=0}^{z}\Big[\frac{d^{\phi}H(t_r, I(t_r))}{\Gamma(\phi+2)}\Big\{(z+1-r)^{\phi}(z+2-r+\phi) - (z-r)^{\phi}(z+2-r+2\phi)\Big\} - \frac{d^{\phi}H(t_{r-1}, I(t_{r-1}))}{\Gamma(\phi+2)}\Big\{(z+1-r)^{\phi+1} - (z-r)^{\phi}(z+1-r+\phi)\Big\}\Big] \tag{41}$$

$$Q(t_{z+1}) = Q(t_0) + \frac{1-\phi}{G(\phi)}H(t_z, Q(t_z)) + \\ + \frac{\phi}{G(\phi)}\sum_{r=0}^{z}\Big[\frac{d^{\phi}H(t_r, Q(t_r))}{\Gamma(\phi+2)}\Big\{(z+1-r)^{\phi}(z+2-r+\phi) - (z-r)^{\phi}(z+2-r+2\phi)\Big\} - \frac{d^{\phi}H(t_{r-1}, Q(t_{r-1}))}{\Gamma(\phi+2)}\Big\{(z+1-r)^{\phi+1} - (z-r)^{\phi}(z+1-r+\phi)\Big\}\Big] \tag{42}$$

$$H(t_{z+1}) = H(t_0) + \frac{1-\phi}{G(\phi)}H(t_z, H(t_z)) + \\ + \frac{\phi}{G(\phi)}\sum_{r=0}^{z}\Big[\frac{d^{\phi}H(t_r, H(t_r))}{\Gamma(\phi+2)}\Big\{(z+1-r)^{\phi}(z+2-r+\phi) - (z-r)^{\phi}(z+2-r+2\phi)\Big\} - \frac{d^{\phi}H(t_{r-1}, H(t_{r-1}))}{\Gamma(\phi+2)}\Big\{(z+1-r)^{\phi+1} - (z-r)^{\phi}(z+1-r+\phi)\Big\}\Big], \tag{43}$$

$$R(t_{z+1}) = R(t_0) + \frac{1-\phi}{G(\phi)}H(t_z, R(t_z)) + \\ + \frac{\phi}{G(\phi)}\sum_{r=0}^{z}\Big[\frac{d^{\phi}H(t_r, R(t_r))}{\Gamma(\phi+2)}\Big\{(z+1-r)^{\phi}(z+2-r+\phi) - (z-r)^{\phi}(z+2-r+2\phi)\Big\} - \frac{d^{\phi}H(t_{r-1}, R(t_{r-1}))}{\Gamma(\phi+2)}\Big\{(z+1-r)^{\phi+1} - (z-r)^{\phi}(z+1-r+\phi)\Big\}\Big], \tag{44}$$

9. Model Fitting and Forecasting

In the present analysis, three continents are targeted to investigate the spread of COVID-19 namely South East Asia, Europe and Americas (North and South America which is considered as a single continent). These three continents are chosen on the basis of high rate of spread of the infection throughout the population. The real data is considered for the period of the last three months i.e., 1st May 2021–31 st July 2021. The reported cases for the selected regions are displayed in the bar chart given in Fig. 2. To match the considered model with the real data, some parameters are found in the literature while some (Table 1) are fitted or estimated. The detail of model fitting for each continent is given below:

9.1. South East Asia

The real reported cases in the south east Asia chosen are between 1st May 2021–31 st July 2021 which are displayed in the bar graph displayed in Fig. 3. Some parameters values are found in the literature while some are estimated or fitted. The fitted model with the real data is portrayed in Fig. 4. According to WHO ("WHO Coronavirus (COVID-19) Dashboard | WHO Coronavirus (COVID-19) Dashboard With Vaccination Data," n.d.), the cases which are reported on 1st May 2021 are 22,280,802 which gradually increases and becomes 38,264,653 on 31st July 2021. The total population of south east Asia for the year 2021 is reported as 655 million ("Southeast Asia - Wikipedia," n.d.). Life expectancy in south east Asia is given as 76.22 years 2021 ("Life expectancy at birth, total (years) - East Asia & Pacific | Data," n.d.). Similarly, other initial conditions are chosen randomly such that exposed individuals are chosen as 6 million, pre-asymptomatic and asymptotic individuals are considered to be 6 million and 4 million respectively. The symptomatic individuals are considered as the total reported cases on 1st May 2021 i.e., 22,280,802. In the same way, quarantined and hospitalized individuals are taken as 5 million and 1 million respectively. While the sum of recovered and removed which is denoted by $R(t)$ are considered as 10 million. The remaining total population is considered to be susceptible which is approximately equal to 600 million. Other parameters are fitted which are given in Table 2. On the basis of table values, the basic reproduction number $\Re_0$ for the spread of COVID-19 in the continent of south east Asia is estimated as 2.8797.

9.2. Europe

The same interval of time for the reported cases is chosen for the case of Europe and the cumulative reported cases are displayed in Fig. 5. According to WHO ("WHO Coronavirus (COVID-19) Dashboard | WHO Coronavirus (COVID-19) Dashboard With Vaccination Data," n.d.), the cases which are reported in Europe on 1st May 2021 are 51,503,191 which rapidly increases up to 60,036,987 at the end of July 2021. The total population of Europe is reported as 746.4 million ("Europe https://data.worldbank.org/indicator/SP.DYN.LE00. IN - Wikipedia," n.d.). Life expectancy in Europe is recorded as 81.06 years ("Life expectancy at birth, total (years) - European Union | Data," n.d.). Similarly, other initial conditions are chosen randomly as the previous case while symptomatic individuals are considered as the total reported cases on 1st May 2021 i.e. 51,503,191. Other parameters are fitted or estimated which are given in Table 3 while the fitted model with the real data is depicted in Fig. 6. On the basis of table values, the basic reproduction number $\Re_0$ for the spread of COVID-19 in the continent of Europe is calculated as 2.23507.

9.3. Americas

The time interval for the spread of COVID-19 is chosen same as the case of Europe and south-east Asia. The cumulative corona virus cases in the continent of Europe for the considered period is portrayed in Fig. 7. According to WHO ("WHO Coronavirus (COVID-19) Dashboard | WHO Coronavirus (COVID-19) Dashboard With Vaccination Data," n.d.), the cases which are reported in America on 1st May 2021 are 62,109,967 which rapidly increases up to 77,003,547 at the end of July 2021. The total population of America for the year 2021 is reported as 1.002 billion ("United States Population, 2021 - Worldometer," n.d.). Life expectancy in America is recorded as 79.11 ("United States of America - Place Explorer - Data Commons," n.d.). Similarly, other initial conditions are chosen randomly as the case of Europe and Asia while the symptomatic individuals are considered as the total reported cases on 1st May 2021. Other parameters are fitted which are given in Table 4. The curve fitting between real data and considered model is displayed in Fig. 8. On the basis of table values, the basic reproduction number $\Re_0$ for the spread of COVID-19 in the continents of Americas is calculated as 2.92819.

10. Results and Discussion

The impact of fractional parameter ϕ on different compartments for the case of south-east Asia is displayed in Fig. 9. Similarly, Figs. 10 and 11 portrays the impact of ϕ on different subclasses for the cases of Europe and America. By varying ϕ while keeping other values fixed, the obtained solutions generate interesting results and gives a variety of solutions of the present model. On the basis of real data reported between 1st May 2021 and 31st July 2021, the results are predicted for the next 200 days. It is noticed that the effect of ϕ is same in all cases i.e., Asia, Europe and Americas. From Fig. 1, it is noticed that by decreasing ϕ, the susceptible individuals $S(t)$ increases which means that less people become exposed. Similarly, increase in $S(t)$ leads to decrease in exposed class and less people becomes exposed by decreasing ϕ. These exposed individuals gradually move to pre-asymptomatic class $A_p(t)$ which is also decreases by decreasing ϕ. Now, there are two routes to move the pre-asymptomatic individuals i.e., Asymptomatic $A(t)$ and symptomatic individuals $I(t)$. Some of pre-asymptomatic individuals move to enter asymptomatic class $A(t)$. It is noticed that $A(t)$ also decreases by decreasing ϕ. Some pre-symptomatic individuals with clear symptoms join the asymptomatic class $I(t)$ where $I(t)$ is also decreases with decrease in ϕ. Furthermore, these symptomatic individuals move to the quarantined $Q(t)$, hospitalized $H(t)$ or recovered/removed class $R(t)$ with different rates. It has been observed that $Q(t)$ and $H(t)$ also decreases by decreasing ϕ because ϕ decreases $I(t)$ which means that there will be not enough infected individuals which move to the $Q(t)$ and $H(t)$. Similarly, recovered or removed individuals $R(t)$ also decreases by decreasing ϕ because all the classes from which the infected individuals move to join the recovered or removed class $R(t)$ decreases with decrease in ϕ.

The variation against ϕ for the dynamics of different compartments for the case of Europe and Americas is same as the case of south-east Asia which is already discussed above. However, some differences are noticed for the case of Asia and Europe. From the figures, it is noticed that the spread of COVID-19 in Asia is comparatively fast to Europe. Similarly, the transmission of disease in Americas is very fast as comparatively to both Europe and Asia. It is also given that the basic reproduction number $\Re_0$ estimated for Asia is high than that of Europe while the basic reproduction number for America is much greater that of the both cases Europe and Asia which is also shown clearly through figures that how the transmission of COVID-19 is high in Americas as compared to the other regions.

The effect of hospitalization rate of symptomatic individuals κ_H on the spread of COVID-19 in different compartment is shown in Fig. 12. It is observed that κ_H dramatically decreases the number of infected individuals over time in the symptomatic class $I(t)$. It means that by increasing the facilities of treatment in public can control the spread of COVID-19. Similarly, it also increases the number of hospitalized individuals $H(t)$ which is obvious. In the same way, κ_H is also responsible in the decrease of $Q(t)$ because most of the infected individuals from $I(t)$ enters to $H(t)$ and there will be not enough individuals left to enter $Q(t)$. Additionally, κ_H also increases the number of susceptible population $S(t)$

Table 2
Fitted Parameters for south-east Asia.

Parameter	Value	Source
μ_A	0.5841	Fitted
μ_{A_P}	0.6233	Fitted
μ_I	0.2346	Fitted
μ_Q	0.1241	Fitted
μ_H	0.1454	Fitted
σ	0.1981	Fitted
ζ	0.6000	Fitted
ψ_A	0.2342	Fitted
ψ_I	0.1223	Fitted
ψ_Q	0.0561	Fitted
κ_Q	0.3345	Fitted
κ_H	0.0634	Fitted
κ_R	0.0145	Fitted
η_R	0.0184	Fitted
β_R	0.0193	Fitted
ψ_R	0.3360	Fitted
λ_R	0.4480	Fitted
Λ	$N(0)\times\delta$	Estimated
δ	$\frac{1}{76.22\times 365}$	("Life expectancy at birth, total (years) - East Asia & Pacific | Data," n.d.)

Table 3
Fitted Parameters for Europe.

Parameter	Value	Source
μ_A	0.5126	Fitted
μ_{A_P}	0.5252	Fitted
μ_I	0.2175	Fitted
μ_Q	0.1126	Fitted
μ_H	0.1526	Fitted
σ	0.1926	Fitted
ζ	0.5982	Fitted
ψ_A	0.2120	Fitted
ψ_I	0.1463	Fitted
ψ_Q	0.0684	Fitted
κ_Q	0.1545	Fitted
κ_H	0.0723	Fitted
κ_R	0.0267	Fitted
η_R	0.0192	Fitted
β_R	0.0294	Fitted
ψ_R	0.3725	Fitted
λ_R	0.4051	Fitted
Λ	$N(0)\times\delta$	Estimated
δ	$\frac{1}{81.06\times 365}$	("Life expectancy at birth, total (years) - European Union | Data," n.d.)

because there will be not enough number of individuals left in symptomatic class $I(t)$ which also decreases the interaction rate between susceptible and infected population which results to keep more people in the susceptible class $S(t)$. As the interaction decreases which results to decrease the spread of virus in overall compartments i.e., $E(t)$, $A_P(t)$ and $A(t)$ because they are dependent to each other. Finally, the effect of κ_H on the recovered population can also be seen from the figure. As, we have already noticed that κ_H decreases the spread as well as interaction among all compartments. So, there will be a smaller number of individuals being infected which means that there will also be a smaller number of individuals become recovered because most of the people will still remain as susceptible.

The effect of quarantine rate of symptomatic individuals κ_Q on the spread of COVID-19 in different compartment is shown in Fig. 13. It has been noticed that κ_Q decreases the number of infected individuals $I(t)$. So, by increasing the awareness of being quarantine among the public, we can better control the spread of COVID-19. Similarly, it also increases the number of quarantined individuals $Q(t)$. κ_Q is also responsible in the decrease of $H(t)$ because most of the infected individuals from $I(t)$ enters to $Q(t)$ and there will be not enough individuals left to enter $H(t)$.

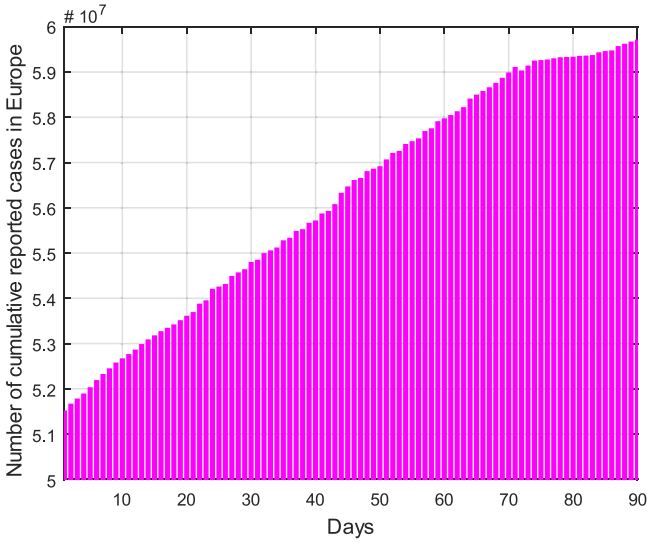

Fig. 5. Cumulative reported cases in Europe between 1st May 2021 and 31st July 2021.

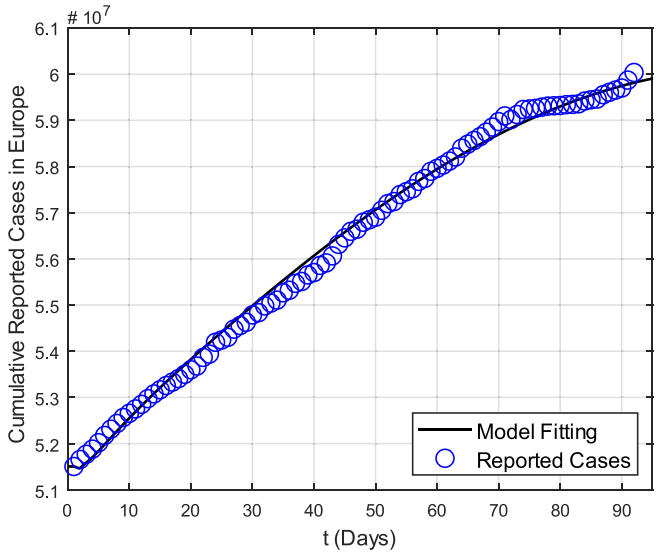

Fig. 6. Model Fitting versus reported cases in Europe between 1st May 2021 and 31st July 2021.

Additionally, κ_Q also increases the number of susceptible population $S(t)$ because there will be not enough number of individuals left in symptomatic class $I(t)$ which also decreases the interaction rate between susceptible and infected population which results to keep more people in the susceptible class $S(t)$. As the interaction decreases which results to decrease the spread of virus in overall compartments i.e., $E(t)$, $A_P(t)$ and $A(t)$ because they are dependent to each other. Finally, the effect of κ_Q on the recovered population can also be seen from the figure. As, we have already noticed that κ_Q decreases the spread as well as interaction among all compartments. So, there will be less number of individuals being infected which means that there will also be less number of individuals become recovered because most of the people will still remain as susceptible.

The quarantine κ_Q parameter and hospitalization parameter κ_H, which are used as the control parameters of COVID-19 in the present analysis. From Figs. 12 and 13, we have observed that a minimal variation in both the quarantine and hospitalization parameters can reduce the spread of infection more quickly. The graphs show that by varying κ_Q

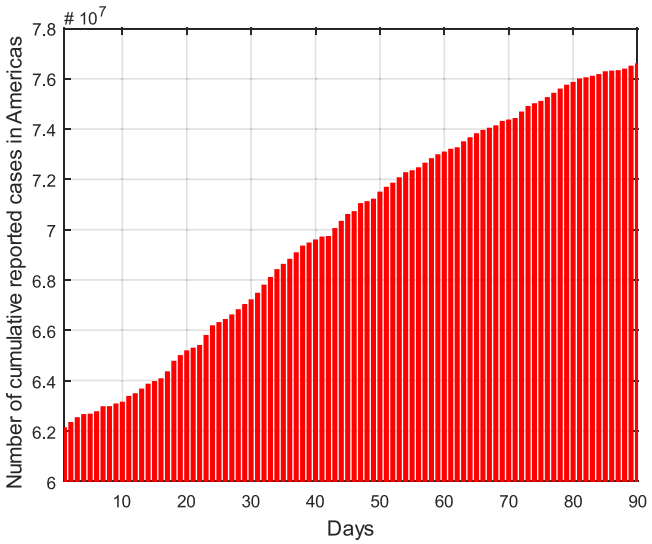

Fig. 7. Cumulative reported cases in Americas between 1st May 2021 and 31st July 2021.

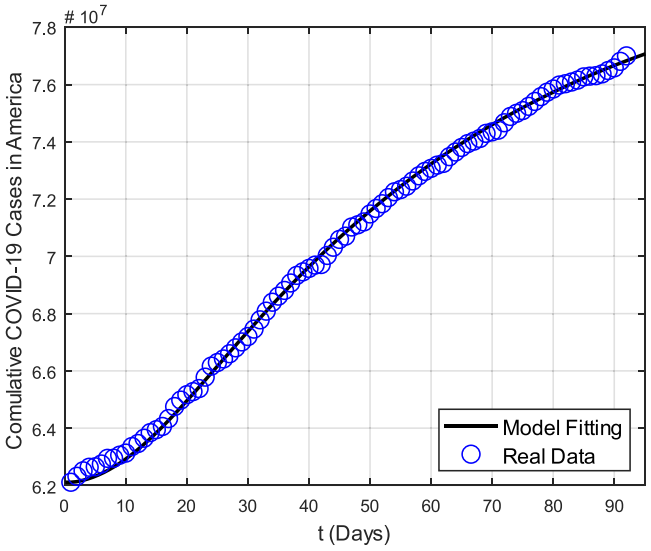

Fig. 8. Model Fitting versus reported cases in Americas between 1st May 2021 and 31st July 2021.

Table 4
Fitted Parameters for Americas.

Parameter	Value	Source
μ_A	0.5148	Fitted
μ_{A_p}	0.6532	Fitted
μ_I	0.1928	Fitted
μ_Q	0.1395	Fitted
μ_H	0.1294	Fitted
σ	0.1029	Fitted
ζ	0.5732	Fitted
ψ_A	0.2253	Fitted
ψ_I	0.1109	Fitted
ψ_Q	0.0534	Fitted
κ_Q	0.3102	Fitted
κ_H	0.0590	Fitted
κ_R	0.0140	Fitted
η_R	0.0178	Fitted
β_R	0.0165	Fitted
ψ_R	0.3778	Fitted
λ_R	0.5487	Fitted
Λ	$N(0) \times \delta$	Estimated
δ	$\frac{1}{79.11 \times 365}$	("United States of America - Place Explorer - Data Commons," n.d.)

and κ_H, it reduces the number of infected individuals dramatically. Hence, if the health authorities aware the people of being quarantine by means of campaign through TV channels, newspapers and social media and also if they facilitate public with a proper treatment, then control of disease can be reduced more quickly.

11. Concluding Remarks

Different mathematical paradigms can provide considerable insights and scientific evidences pertinent to any ongoing epidemic dynamics. Based on those valuable information, health officials and public health-experts can set up potential control strategies to battle against any epidemic. From the emergence of the novel coronavirus in China, researchers and scientists are working relentlessly to develop various mathematical modeling approaches to gain a deeper understanding on the progression dynamics of COVID-19 in the world. On the basis of robust forecasting results of reliable epidemiological models, government officials can deploy different public health intervention strategies to control the rapid transmission of the virus. Herein, the dynamics and transmission of COVID-19 is predicted for the next 200 days. Based on the fitted values of parameters, the basic reproduction number $\Re_0$ for the case of America, Asia and Europe is$\Re_0 \approx 2.92819$, $\Re_0 \approx 2.87970$ and $\Re_0 \approx 2.23507$ respectively. This means that the spread of COVID-19 in America is high which is follower by Asia and Europe. Basic Reproduction number is very crucial number through which we can find that the disease is an endemic or it will vanish and approach to it disease free equilibrium. Here, the basic reproduction number is between 2 and 3 for all the considered regions which means that every infected individual will infect at least 2–3 susceptible individuals and the disease dynamics will approach to endemic state because $\Re_0 > 1$. Our data indicates that awareness of being quarantined and proper treatment can minimize the virus risk. the number of infected cases is expected to decrease in a faster way if governments continue to adhere to COVID-19 restrictions and control measures. We believe that if the government restricts people to their homes only, avoids shaking hands, follows proper hand washing procedures, limits visits to endemic areas, restricts places where infection can be spread further, and carefully monitors physical and social distances, the number of infected cases will reduce more quickly.

This work can be extended in different directions such as by including different classes of human population be categorized the population via age wise or gender or characteristic wise. Moreover, the present problem can be analyzed through a different numerical or analytical technique. The idea of different fractional operators such as Caputo, Caputo-Fabrizio, generalized Caputo or AB or Prabhakar type fractional operators can be utilized and the results can be compared to show that which type of fractional operator can give us the best results. The idea of different fractal-fractional operators of different kernels can be implemented to the existing model. In addition to that, this model can be used for a different area, location or the data of different time interval can be used. This model can also be linked to other diseases through the co-infection model. Different incidence rates such as generalized, bilinear, saturated or half saturated type or many others can be used.

Declaration of Competing Interest

The authors declare that they have no known competing financial interests or personal relationships that could have appeared to influence the work reported in this paper.

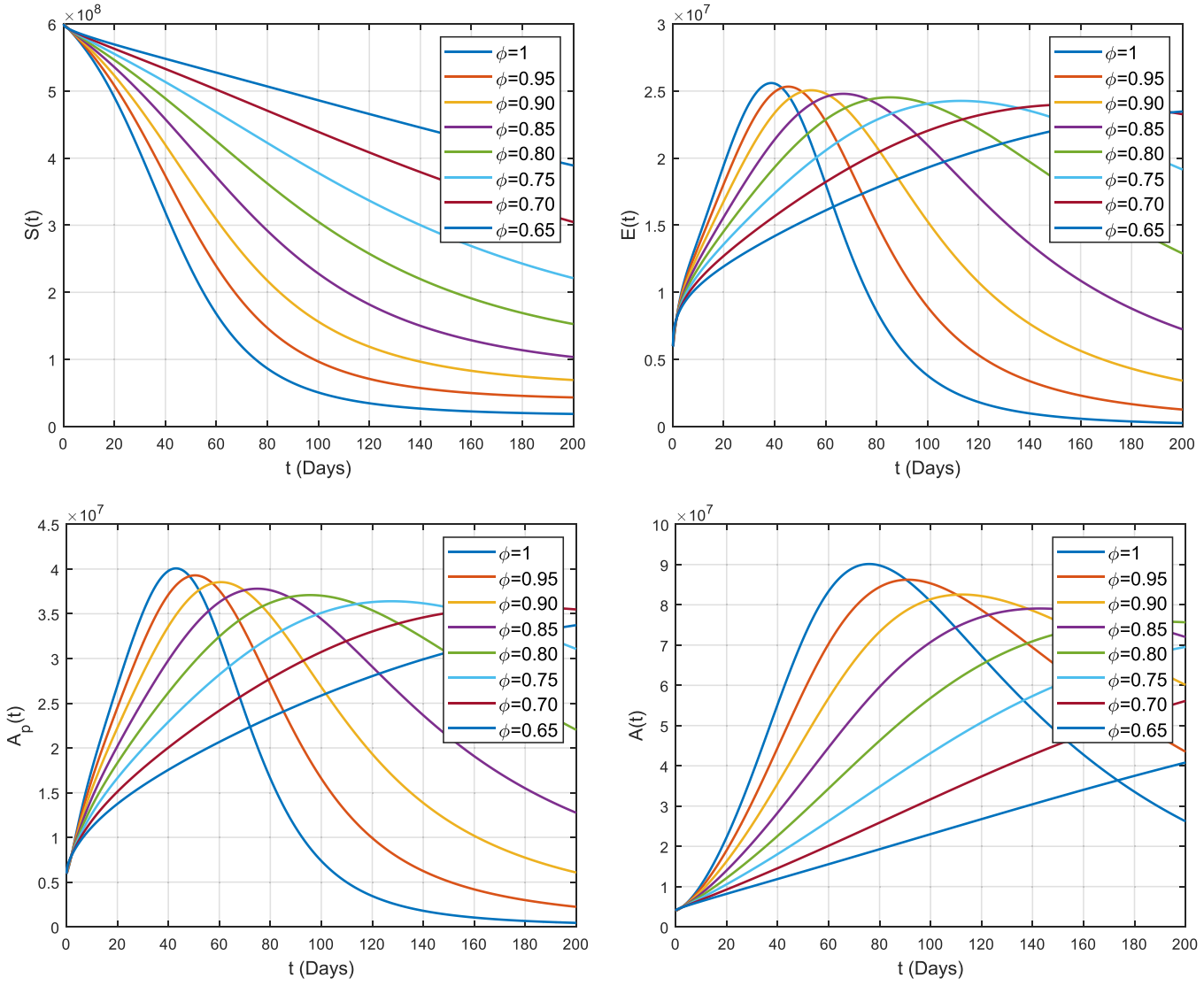

Fig. 9. Impact of fractional parameter ϕ on the dynamics of COVID-19 among different compartments in south-east Asia.

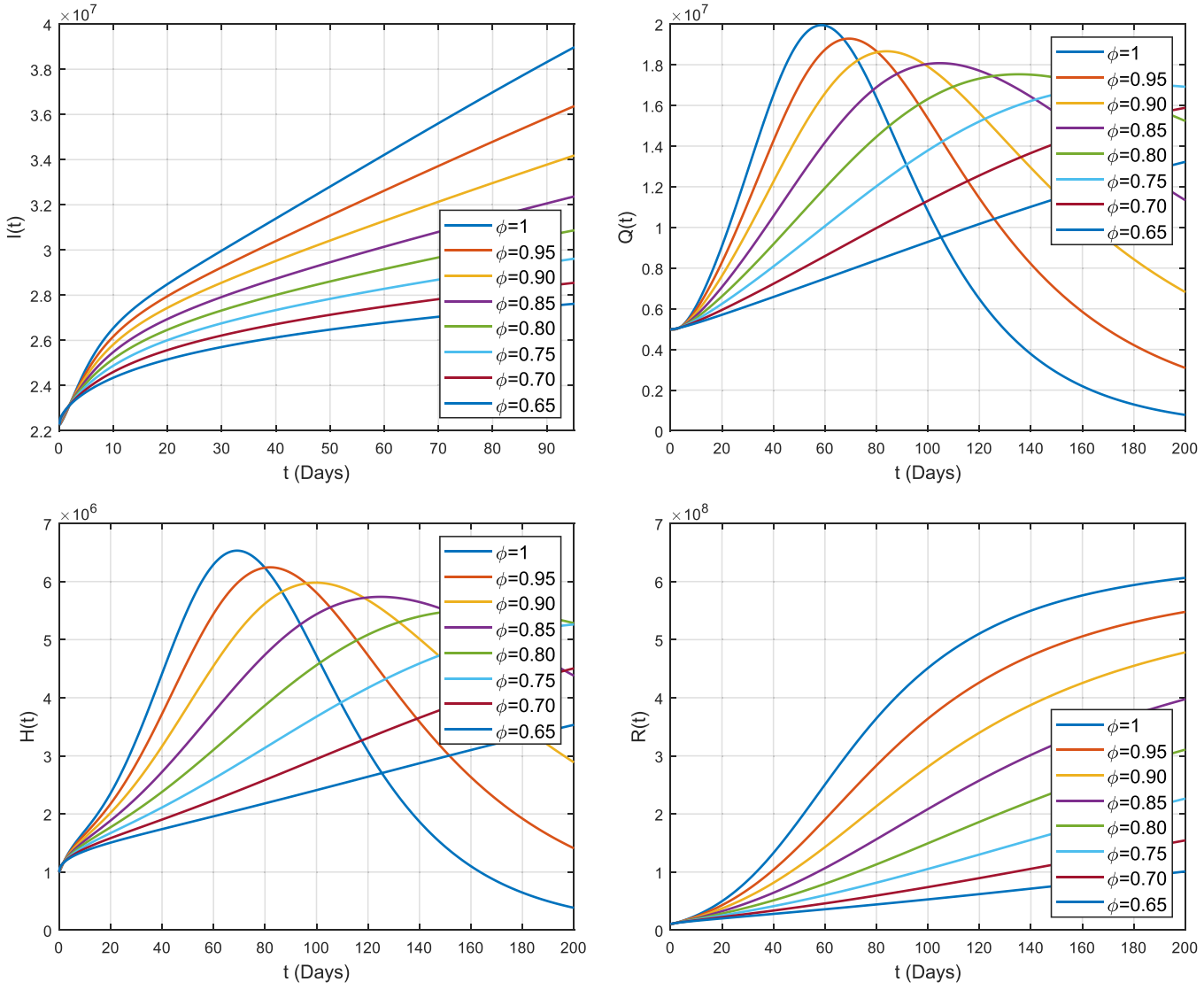

Fig. 9. (*continued*).

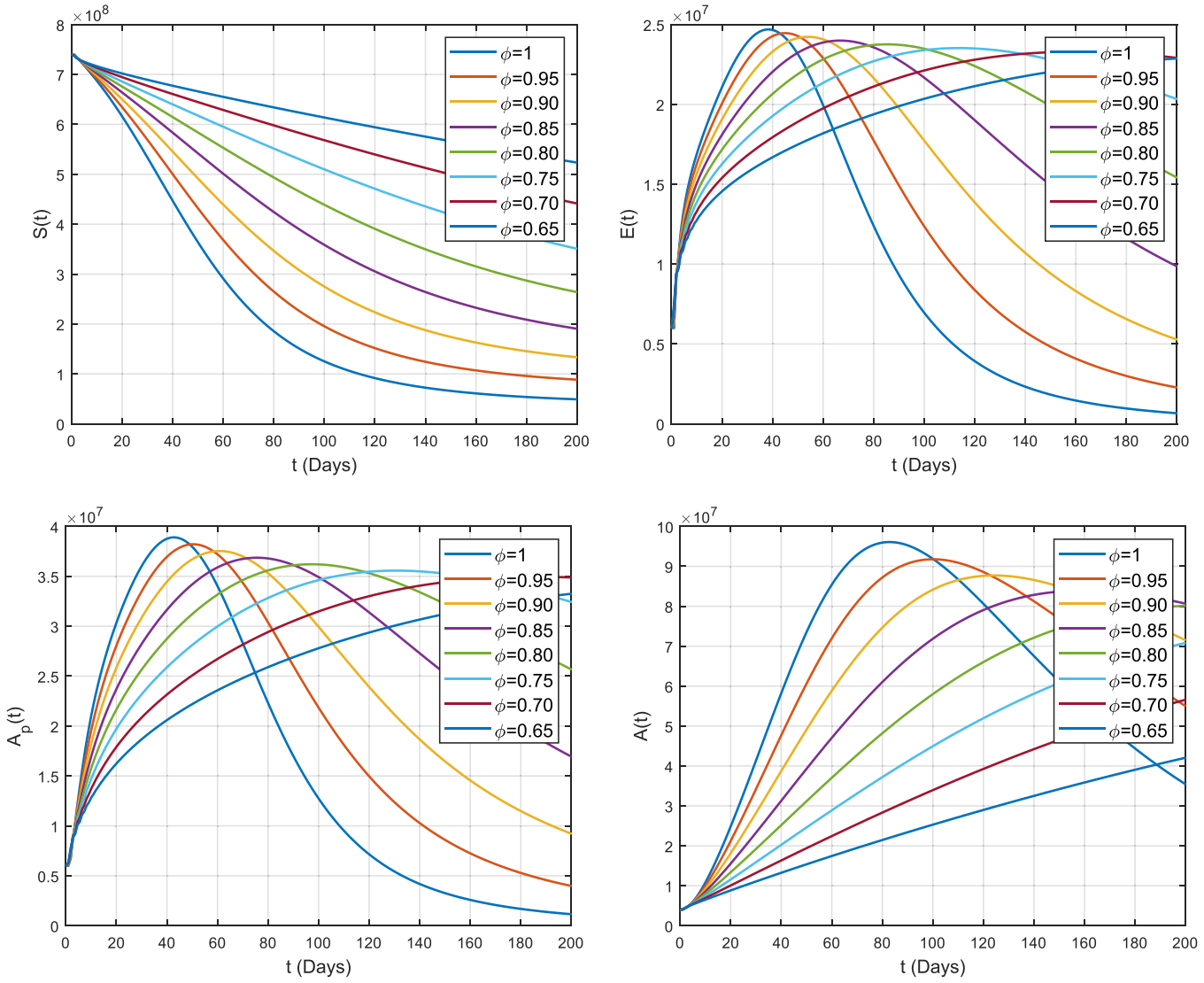

Fig. 10. Impact of fractional parameter ϕ on the dynamics of COVID-19 among different compartments in Europe.

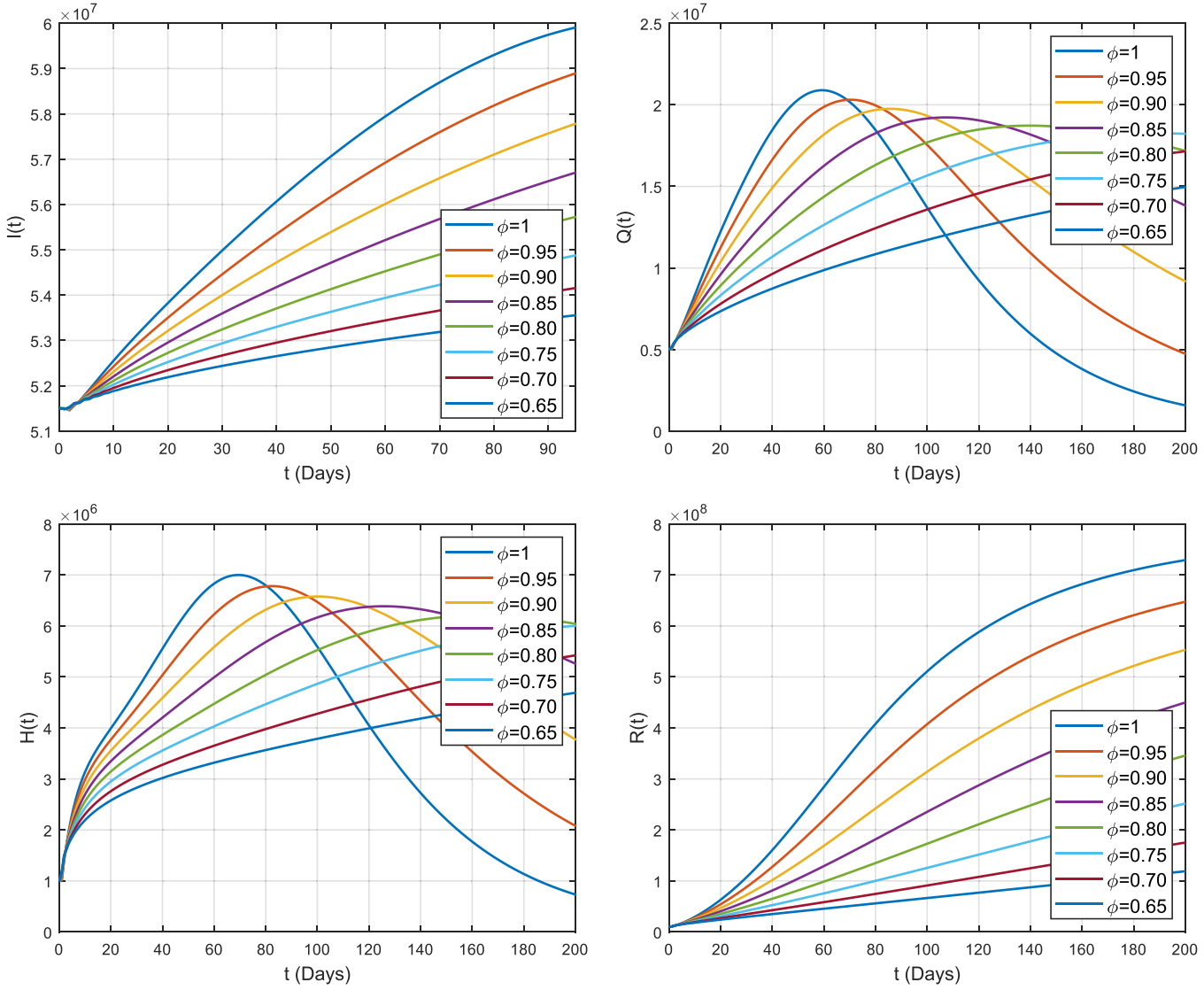

Fig. 10. (*continued*).

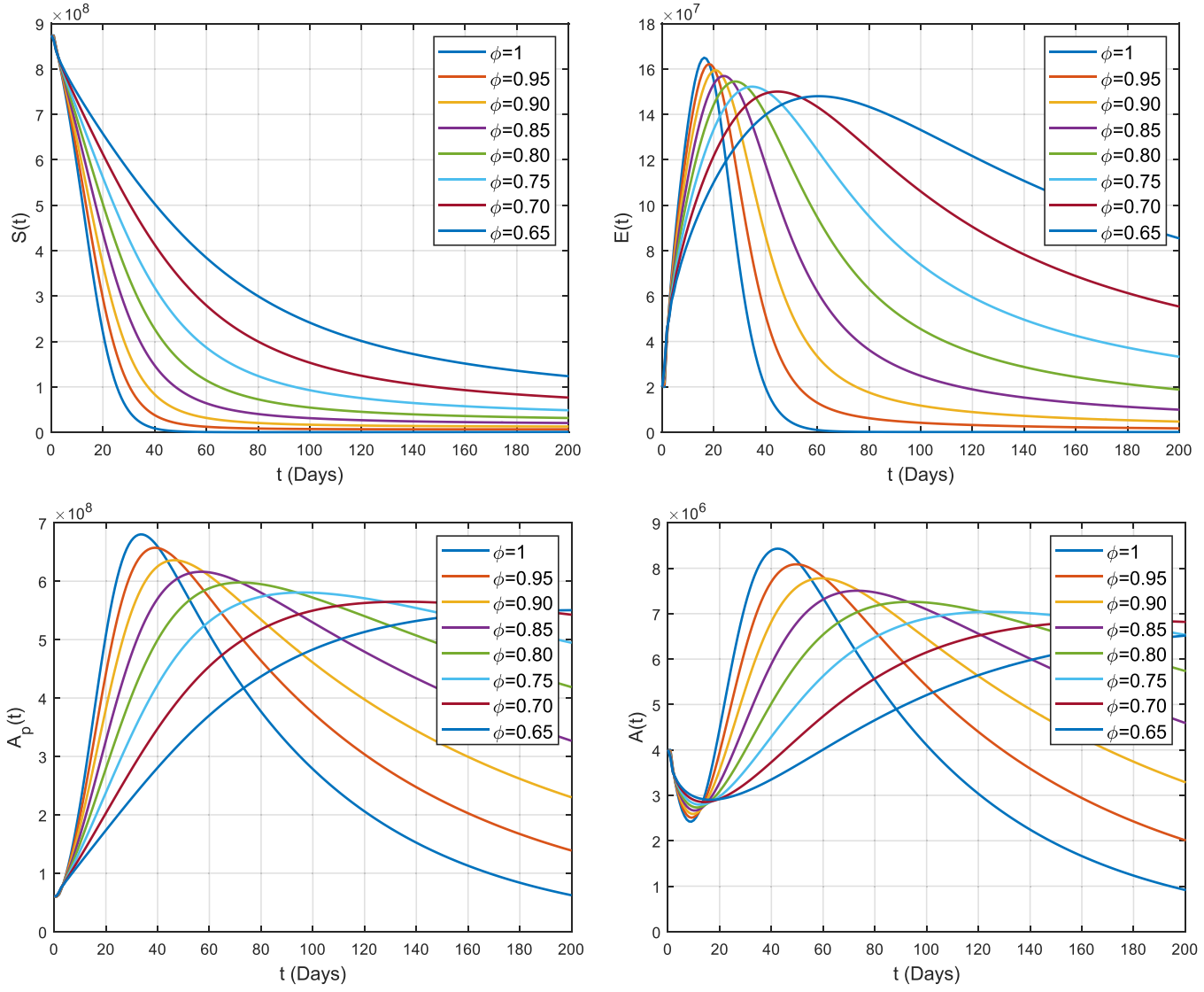

Fig. 11. Impact of fractional parameter ϕ on the dynamics of COVID-19 among different compartments in Americas.

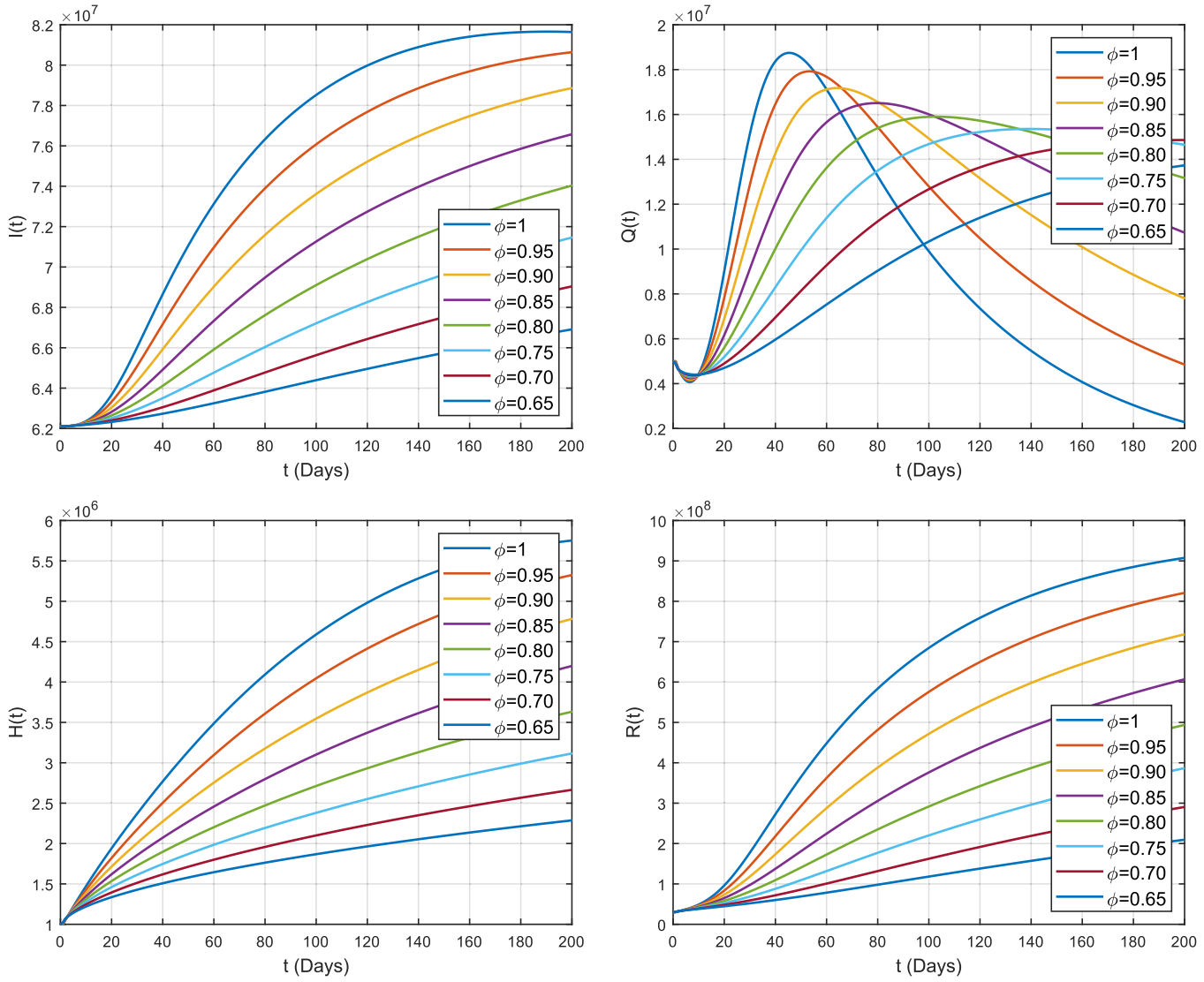

Fig. 11. (*continued*).

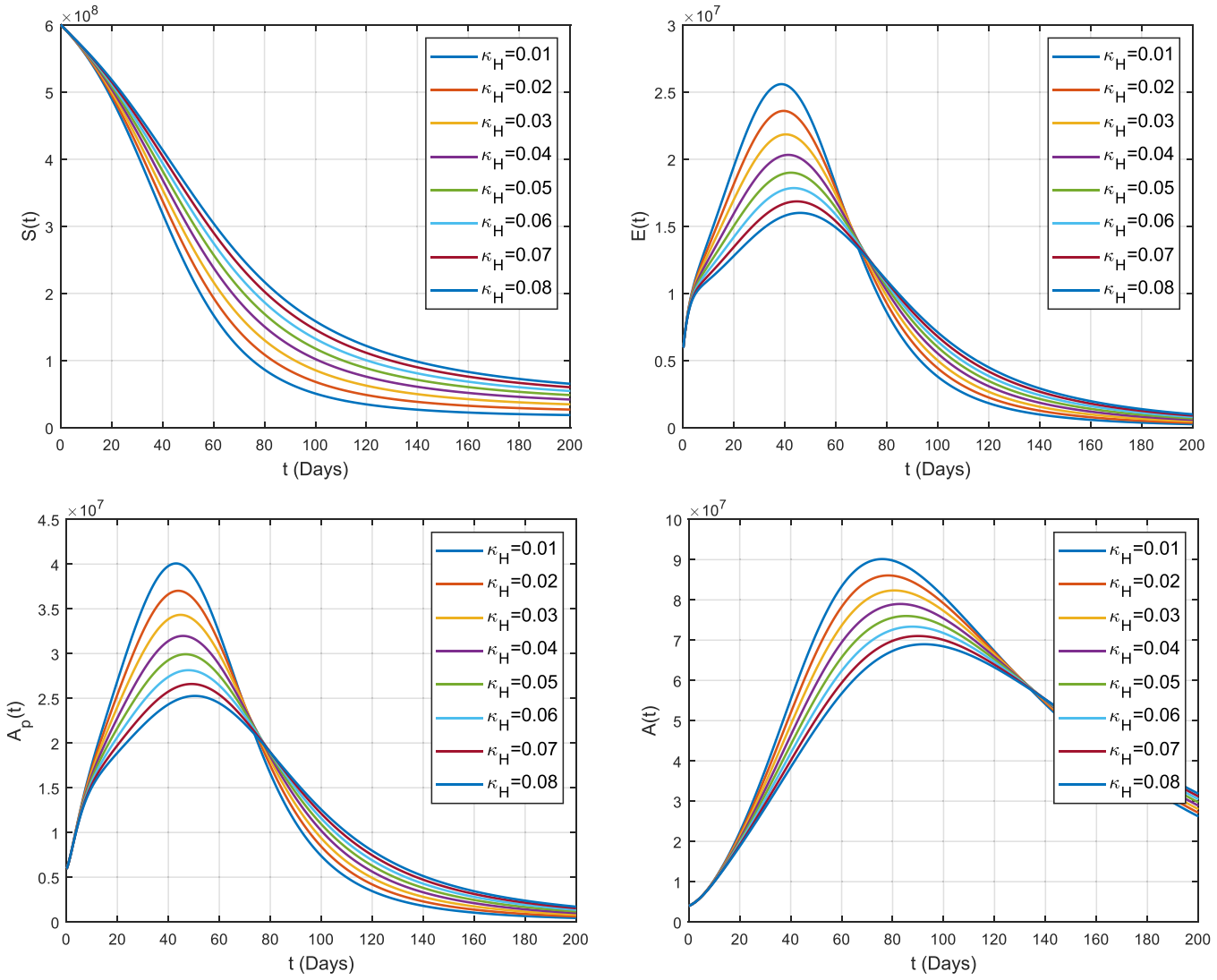

Fig. 12. Impact of rate of hospitalization κ_H on the dynamics of COVID-19 among different compartments.

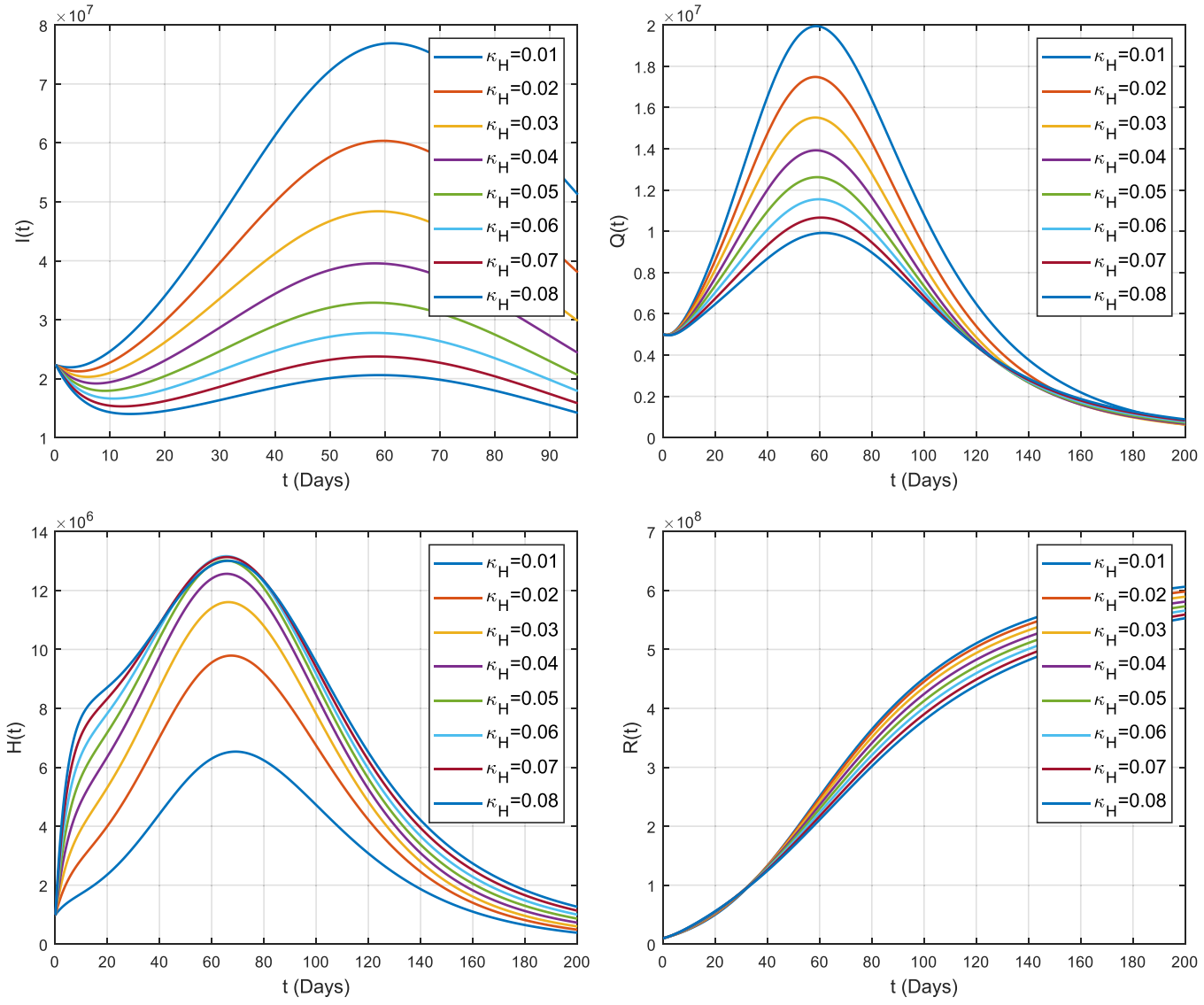

Fig. 12. (*continued*).

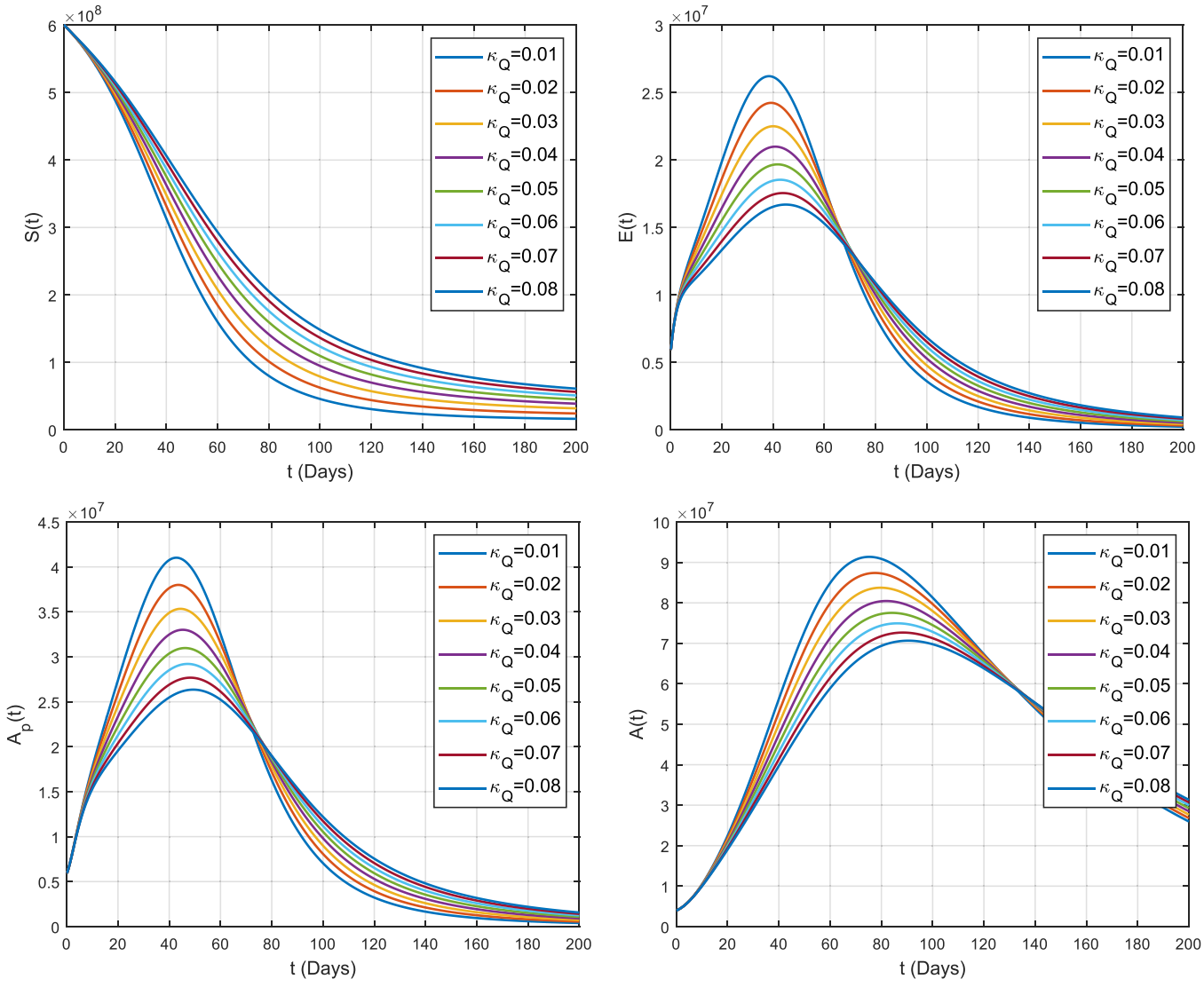

Fig. 13. Impact of rate of quarantine κ_Q on the dynamics of COVID-19 among different compartments.

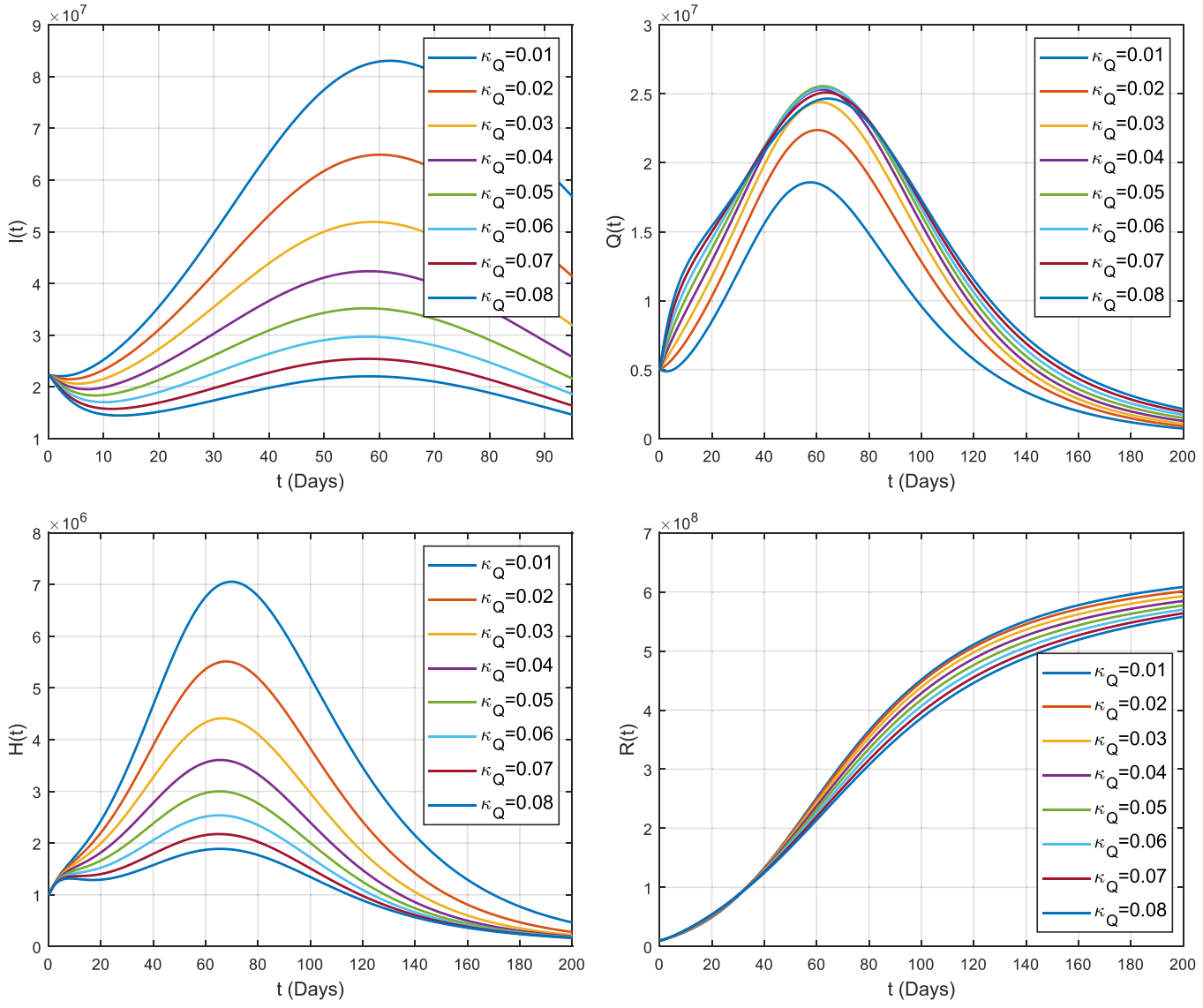

Fig. 13. (*continued*).

Acknowledgements

The authors acknowledge the generous charitable donation from the late Sheikh Ibraheem Ahmed Azhar as a contribution to the scientific research community.

References

Aba Oud, M.A., Ali, A., Alrabaiah, H., Ullah, S., Khan, M.A., Islam, S., 2021. A fractional order mathematical model for COVID-19 dynamics with quarantine, isolation, and environmental viral load. Adv. Differ. Eqs. 2021, 1–19. https://doi.org/10.1186/S13662-021-03265-4/FIGURES/9.

Agusto, F.B., Khan, M.A., 2018. Optimal control strategies for dengue transmission in pakistan. Math. Biosci. 305, 102–121. https://doi.org/10.1016/J.MBS.2018.09.007.

Ahmad, Abdullah, Owyed, S., Abdel-Aty, S., Mahmoud, A.H., Shah, E.E., K. Alrabaiah, H., 2021. Mathematical analysis of COVID-19 via new mathematical model. Chaos, Solitons Fractals 143, 110585. https://doi.org/10.1016/J.CHAOS.2020.110585.

Ahmad, S., Ullah, A., Al-Mdallal, Q.M., Khan, H., Shah, K., Khan, A., 2020. Fractional order mathematical modeling of COVID-19 transmission. Chaos, Solitons Fractals 139, 110256. https://doi.org/10.1016/J.CHAOS.2020.110256.

Ahmad, S.W., Sarwar, M., Rahmat, G.U.L., Shah, K., Ahmad, H., Mousa, A.A.A., 2021. Fractional order model for the CORONAVIRUS (COVID-19) in Wuhan. CHINA 30, 2240007. https://doi.org/10.1142/S0218348×22400072.

Ahmad, z, Ali, F., Alqahtani, A.M., Khan, N., Khan, I., 2021. Dyn. Coop. React. Based Chem. Kinet. React. Speed.: a Comp. Anal. Singul. nonsingular Kernels. https://doi.org/10.1142/S0218348×22400485.

Ahmad, Z., Arif, M., Khan, I., 2020b. Dynamics of fractional order sir model with a case study of COVID-19 in Turkey. City Univ. Int. J. Comput. Anal. 4, 19–37. https://doi.org/10.33959/CUIJCA.V4I01.43.

Ahmad, Z., Ali, F., Khan, N., Khan, I., 2021. Dynamics of fractal-fractional model of a new chaotic system of integrated circuit with Mittag-Leffler kernel. Chaos, Solitons Fractals 153, 111602. https://doi.org/10.1016/J.CHAOS.2021.111602.

Ahmad, Z., Arif, M., Ali, F., Khan, I., Nisar, K.S., 2020a. A report on COVID-19 epidemic in Pakistan using SEIR fractional model. Sci. Rep. 2020 (101 10), 1–14. https://doi.org/10.1038/s41598-020-79405-9.

Ali, A., Iqbal, Q., Asamoah, J.K.K., Islam, S., 2022a. Mathematical modeling for the transmission potential of Zika virus with optimal control strategies. Eur. Phys. J. 2022 (1371 137), 1–30. https://doi.org/10.1140/EPJP/S13360-022-02368-5.

Ali, A., Islam, S., Khan, M.R., Rasheed, S., Allehiany, F.M., Baili, J., Khan, M.A., Ahmad, H., 2022b. Dynamics of a fractional order Zika virus model with mutant. Alex. Eng. J. 61, 4821–4836. https://doi.org/10.1016/J.AEJ.2021.10.031.

Ali, F., Ahmad, Z., Arif, M., Khan, I., Nisar, K.S., 2020. A time fractional model of generalized couette flow of couple stress nanofluid with heat and mass transfer: applications in engine oil. IEEE Access 8, 146944–146966. https://doi.org/10.1109/ACCESS.2020.3013701.

Arfan, M., Shah, K., Abdeljawad, T., Mlaiki, N., Ullah, A., 2021. A Caputo power law model predicting the spread of the COVID-19 outbreak in Pakistan. Alex. Eng. J. 60, 447–456. https://doi.org/10.1016/J.AEJ.2020.09.011.

Atangana, A., 2017. Fractal-fractional differentiation and integration: Connecting fractal calculus and fractional calculus to predict complex system. Chaos, Solitons Fractals 102, 396–406. https://doi.org/10.1016/J.CHAOS.2017.04.027.

Atangana, A., Baleanu, D., 2016. New fractional derivatives with nonlocal and non-singular kernel: theory and application to heat transfer model. Therm. Sci. 20, 763–769.

Atangana, A., İğret Araz, S., 2021. Modeling and forecasting the spread of COVID-19 with stochastic and deterministic approaches: Africa and Europe, 2021 20211 2021 Adv. Differ. Equ. 1–107. https://doi.org/10.1186/S13662-021-03213-2.

Bendavid, E., Oh, C., Bhattacharya, J., Ioannidis, J.P.A., 2021. Assessing mandatory stay-at-home and business closure effects on the spread of COVID-19. Eur. J. Clin. Invest 51, e13484. https://doi.org/10.1111/ECI.13484.

Burki, T., 2020. China's successful control of COVID-19. Lancet Infect. Dis. 20, 1240–1241. https://doi.org/10.1016/S1473-3099(20)30800-8.

Danane, J., Allali, K., Hammouch, Z., Nisar, K.S., 2021. Mathematical analysis and simulation of a stochastic COVID-19 Lévy jump model with isolation strategy. Results Phys. 23, 103994 https://doi.org/10.1016/J.RINP.2021.103994.

Grassly, N.C., Pons-Salort, M., Parker, E.P.K., White, P.J., Ferguson, N.M., Ainslie, K., Baguelin, M., Bhatt, S., Boonyasiri, A., Brazeau, N., Cattarino, L., Coupland, H., Cucunuba, Z., Cuomo-Dannenburg, G., Dighe, A., Donnelly, C., van Elsland, S.L., FitzJohn, R., Flaxman, S., Fraser, K., Gaythorpe, K., Green, W., Hamlet, A., Hinsley, W., Imai, N., Knock, E., Laydon, D., Mellan, T., Mishra, S., Nedjati-Gilani, G., Nouvellet, P., Okell, L., Ragonnet-Cronin, M., Thompson, H.A., Unwin, H. J.T., Vollmer, M., Volz, E., Walters, C., Wang, Y., Watson, O.J., Whittaker, C., Whittles, L., Xi, X., 2020. Comparison of molecular testing strategies for COVID-19 control: a mathematical modelling study. Lancet Infect. Dis. 20, 1381–1389. https://doi.org/10.1016/S1473-3099(20)30630-7.

Grigorieva, E., Khailov, E., Korobeinikov, A., 2020. Optimal quarantine strategies for COVID-19 control models.

Jin, Y., Yang, H., Ji, W., Wu, W., Chen, S., Zhang, W., Duan, G., 2020. Virology, Epidemiology, Pathogenesis, and Control of COVID-19, 372 12 Viruses 2020 Vol. 12, 372. https://doi.org/10.3390/V12040372.

Kassa, S.M., Njagarah, J.B.H., Terefe, Y.A., 2020. Analysis of the mitigation strategies for COVID-19: From mathematical modelling perspective. Chaos, Solitons Fractals 138, 109968. https://doi.org/10.1016/J.CHAOS.2020.109968.

Khajanchi, S., Sarkar, K., 2020. Forecasting the daily and cumulative number of cases for the COVID-19 pandemic in India. Chaos Interdiscip. J. Nonlinear Sci. 30, 071101 https://doi.org/10.1063/5.0016240.

Khajanchi, S., Sarkar, K., Mondal, J., 2020. Dynamics of the COVID-19 pandemic in India. https://doi.org/10.21203/rs.3.rs-27112/v1.

Khajanchi, S., Bera, S., Roy, T.K., 2021a. Mathematical analysis of the global dynamics of a HTLV-I infection model, considering the role of cytotoxic T-lymphocytes. Math. Comput. Simul. 180, 354–378. https://doi.org/10.1016/J.MATCOM.2020.09.009.

Khajanchi, S., Sarkar, K., Mondal, J., Nisar, K.S., Abdelwahab, S.F., 2021b. Mathematical modeling of the COVID-19 pandemic with intervention strategies. Results Phys. 25, 104285 https://doi.org/10.1016/J.RINP.2021.104285.

Khan, M.A., Atangana, A., 2020. Modeling the dynamics of novel coronavirus (2019-nCov) with fractional derivative. Alex. Eng. J. 59, 2379–2389. https://doi.org/10.1016/J.AEJ.2020.02.033.

Kucharski, A.J., Russell, T.W., Diamond, C., Liu, Y., Edmunds, J., Funk, S., Eggo, R.M., Sun, F., Jit, M., Munday, J.D., Davies, N., Gimma, A., van Zandvoort, K., Gibbs, H., Hellewell, J., Jarvis, C.I., Clifford, S., Quilty, B.J., Bosse, N.I., Abbott, S., Klepac, P., Flasche, S., 2020. Early dynamics of transmission and control of COVID-19: a mathematical modelling study. Lancet Infect. Dis. 20, 553–558. https://doi.org/10.1016/S1473-3099(20)30144-4/ATTACHMENT/60AE6635-8A55-49D0-A2CE-31F41FC9FBA2/MMC1.PDF.

Memon, Z., Qureshi, S., Memon, B.R., 2021. Assessing the role of quarantine and isolation as control strategies for COVID-19 outbreak: a case study. Chaos, Solitons Fractals 144, 110655. https://doi.org/10.1016/J.CHAOS.2021.110655.

Murtaza, S., Kumam, P., Ahmad, Z., Seangwattana, T., Ali, I.E., 2022. Numerical Analysis of Newley Developed Fractal-Fractional Model of Casson Fluid with Exponential Memory. Fractals. https://doi.org/10.1142/S0218348×2240151X.

Naik, P.A., Yavuz, M., Qureshi, S., Zu, J., Townley, S., 2020. Modeling and analysis of COVID-19 epidemics with treatment in fractional derivatives using real data from Pakistan. Eur. Phys. J. 2020 (13510 135), 1–42. https://doi.org/10.1140/EPJP/S13360-020-00819-5.

Nisar, K.S., Ahmad, S., Ullah, A., Shah, K., Alrabaiah, H., Arfan, M., 2021. Mathematical analysis of SIRD model of COVID-19 with Caputo fractional derivative based on real data. Results Phys. 21, 103772 https://doi.org/10.1016/J.RINP.2020.103772.

Pellis, L., Scarabel, F., Stage, H.B., Overton, C.E., Chappell, L.H.K., Fearon, E., Bennett, E., Lythgoe, K.A., House, T.A., Hall, I., Group, U. of M.C.-19 M, 2021. Challenges in control of COVID-19: short doubling time and long delay to effect of interventions. Philos. Trans. R. Soc. B 376. https://doi.org/10.1098/RSTB.2020.0264.

Qureshi, S., Atangana, A., 2019. Mathematical analysis of dengue fever outbreak by novel fractional operators with field data. Phys. A Stat. Mech. its Appl. 526, 121127 https://doi.org/10.1016/J.PHYSA.2019.121127.

Qureshi, S., Yusuf, A., 2019a. Modeling chickenpox disease with fractional derivatives: from caputo to atangana-baleanu. Chaos, Solitons Fractals 122, 111–118. https://doi.org/10.1016/J.CHAOS.2019.03.020.

Qureshi, S., Yusuf, A., 2019b. Fractional derivatives applied to MSEIR problems: Comparative study with real world data. Eur. Phys. J. 2019 (1344 134), 1–13. https://doi.org/10.1140/EPJP/I2019-12661-7.

Qureshi, S., Yusuf, A., 2019c. Fractional derivatives applied to MSEIR problems: Comparative study with real world data. Eur. Phys. J. 2019 (1344 134), 1–13. https://doi.org/10.1140/EPJP/I2019-12661-7.

Qureshi, S., Bonyah, E., Shaikh, A.A., 2019a. Classical and contemporary fractional operators for modeling diarrhea transmission dynamics under real statistical data. Phys. A Stat. Mech. its Appl. 535, 122496 https://doi.org/10.1016/J.PHYSA.2019.122496.

Qureshi, S., Yusuf, A., Shaikh, A.A., Inc, M., 2019b. Transmission dynamics of varicella zoster virus modeled by classical and novel fractional operators using real statistical data. Phys. A Stat. Mech. its Appl. 534, 122149 https://doi.org/10.1016/J.PHYSA.2019.122149.

Rai, R.K., Khajanchi, S., Tiwari, P.K., Venturino, E., Misra, A.K., 2022. Impact of social media advertisements on the transmission dynamics of COVID-19 pandemic in India. J. Appl. Math. Comput. 68, 19–44. https://doi.org/10.1007/S12190-021-01507-Y/FIGURES/9.

Rajagopal, K., Hasanzadeh, N., Parastesh, F., Hamarash, I.I., Jafari, S., Hussain, I., 2020. A fractional-order model for the novel coronavirus (COVID-19) outbreak. Nonlinear Dyn. 2020 1011 101, 711–718. https://doi.org/10.1007/S11071-020-05757-6.

Samui, P., Mondal, J., Khajanchi, S., 2020. A mathematical model for COVID-19 transmission dynamics with a case study of India. Chaos, Solitons Fractals 140, 110173. https://doi.org/10.1016/J.CHAOS.2020.110173.

Sánchez, Y.G., Sabir, Z., Guirao, J.L.G., 2020. Des. a Nonlinear Sitr Fractal Model Based Dyn. a Nov. Corona (COVID-19) 12, 2040026. https://doi.org/10.1142/S0218348×20400265.

Sarkar, K., Khajanchi, S., Nieto, J.J., 2020. Modeling and forecasting the COVID-19 pandemic in India. Chaos, Solitons Fractals 139, 110049. https://doi.org/10.1016/J.CHAOS.2020.110049.

Sene, N., 2020. SIR epidemic model with Mittag–Leffler fractional derivative. Chaos, Solitons Fractals 137, 109833. https://doi.org/10.1016/J.CHAOS.2020.109833.

Shah, K., Abdeljawad, T., Mahariq, I., Jarad, F., Deniz, S., 2020. Qualitative Analysis of a Mathematical Model in the Time of COVID-19. Biomed. Res. Int 2020. https://doi.org/10.1155/2020/5098598.

Shaikh, A.S., Shaikh, I.N., Nisar, K.S., 2020. A mathematical model of COVID-19 using fractional derivative: outbreak in India with dynamics of transmission and control. Adv. Differ. Eqs. 2020, 1–19. https://doi.org/10.1186/S13662-020-02834-3/FIGURES/6.

Sharomi, O., Malik, T., 2017. Optimal control in epidemiology. Ann. Oper. Res. 251, 55–71. https://doi.org/10.1007/S10479-015-1834-4.

Shatanawi, W., Abdo, M.S., Abdulwasaa, M.A., Shah, K., Panchal, S.K., Kawale, S.V., Ghadle, K.P., 2021. A fractional dynamics of tuberculosis (TB) model in the frame of generalized Atangana–Baleanu derivative. Results Phys. 29, 104739 https://doi.org/10.1016/J.RINP.2021.104739.

Sinan, M., Shah, K., Kumam, P., Mahariq, I., Ansari, K.J., Ahmad, Z., Shah, Z., 2021. Fractional order mathematical modelling of typhoid fever disease. Results Phys. 32, 105044 https://doi.org/10.1016/j.rinp.2021.105044.

Sinan, M., Ahmad, H., Ahmad, Z., Baili, J., Murtaza, S., Aiyashi, M.A., Botmart, T., 2022. Fractional mathematical modeling of malaria disease with treatment & insecticides. Results Phys. 34, 105220 https://doi.org/10.1016/J.RINP.2022.105220.

Singh, H., Srivastava, H.M., Hammouch, Z., Sooppy Nisar, K., 2021. Numerical simulation and stability analysis for the fractional-order dynamics of COVID-19. Results Phys. 20, 103722 https://doi.org/10.1016/J.RINP.2020.103722.

Tiwari, P.K., Rai, R.K., Khajanchi, S., Gupta, R.K., Misra, A.K., 2021. Dynamics of coronavirus pandemic: effects of community awareness and global information campaigns. Eur. Phys. J. 2021 (13610 136), 1–23. https://doi.org/10.1140/EPJP/S13360-021-01997-6.

Toufik, M., Atangana, A., 2017. New numerical approximation of fractional derivative with non-local and non-singular kernel: application to chaotic models. Eur. Phys. J. 2017 (13210 132), 1–16. https://doi.org/10.1140/EPJP/I2017-11717-0.

United States Population (2021) - Worldometer [WWW Document], n.d. URL https://www.worldometers.info/world-population/us-population/ (Accessed 9 February 2021).

Van Den Driessche, P., Watmough, J., 2002a. Reproduction numbers and sub-threshold endemic equilibria for compartmental models of disease transmission. Math. Biosci. 180, 29–48. https://doi.org/10.1016/S0025-5564(02)00108-6.

Van Den Driessche, P., Watmough, J., 2002b. Reproduction numbers and sub-threshold endemic equilibria for compartmental models of disease transmission. Math. Biosci. 180, 29–48. https://doi.org/10.1016/S0025-5564(02)00108-6.

Wu, J.T., Leung, K., Bushman, M., Kishore, N., Niehus, R., de Salazar, P.M., Cowling, B.J., Lipsitch, M., Leung, G.M., 2020. Estimating clinical severity of COVID-19 from the transmission dynamics in Wuhan, China. Nat. Med. 2020 (264 26), 506–510. https://doi.org/10.1038/s41591-020-0822-7.

Yadav, R.P., Renu, V., 2020. A numerical simulation of fractional order mathematical modeling of COVID-19 disease in case of Wuhan China. Chaos Solitons Fractals 140, 110124. https://doi.org/10.1016/j.chaos.2020.110124. Epub 2020/08/25. PubMed PMID: 32834636; PubMed Central PMCID: PMCPMC7365131.

Yavuz, M., Özdemir, N., 2019. Comparing the new fractional derivative operators involving exponential and Mittag-Leffler kernel. Vol. 13, Pages 995-1006 13 Discret. Contin. Dyn. Syst. - S. 2020, 995. https://doi.org/10.3934/DCDSS.2020058.

Yusuf, A., Qureshi, S., Feroz Shah, S., 2020. Mathematical analysis for an autonomous financial dynamical system via classical and modern fractional operators. Chaos, Solitons Fractals 132, 109552. https://doi.org/10.1016/J.CHAOS.2019.109552.

Zamir, M., Shah, Z., Nadeem, F., Memood, A., Alrabaiah, H., Kumam, P., 2020. Non pharmaceutical interventions for optimal control of COVID-19. Comput. Methods Prog. Biomed. 196, 105642 https://doi.org/10.1016/J.CMPB.2020.105642.

Zhao, S., Chen, H., 2020. Modeling the epidemic dynamics and control of COVID-19 outbreak in China. Quant. Biol. (Beijing, China) 8, 1. https://doi.org/10.1007/S40484-020-0199-0.